

Chapter 2

Morphological Image Analysis for Computer Vision Applications

Y.V. Vizilter, Y.P. Pyt'ev, A.I. Chulichkov and L.M. Mestetskiy

Abstract Some original and novel morphological concepts and tools are presented in this chapter as well as required amount of mathematical morphological basics. The continuous binary morphology based on a computational geometry is presented as a very fast approach to shape representation via real-time computation of figures' skeletons. A skeletal representation of the figure is formed as a skeleton graph, and the radial function is determined in skeleton points. The proposed morphological spectrum is the multi-scale morphological shape description and analysis tools based on granulometry. It is shown how the tasks of change detection and shape matching in images can be solved using a morphological image analysis. The projective morphology as a generalized framework based on the mathematical morphology and the morphological image analysis provides fast and efficient solutions of morphological segmentation problem in complex images.

Keywords Mathematical morphology • Shape representation • Continuous skeleton • Morphological spectrum • Image analysis • Change detection • Image matching • Image segmentation

Y.V. Vizilter (✉)

State Research Institute of Aviation Systems, 7, Viktorenko str., Moscow 125319,
Russian Federation
e-mail: viz@gosniias.ru

Y.P. Pyt'ev • A.I. Chulichkov

M.V. Lomonosov Moscow State University, 1, Leninskie Gory, Moscow 119991,
Russian Federation
e-mail: achulichkov@gmail.ru

L.M. Mestetskiy

Moscow International University, 17, Leningradsky av., Moscow 125040,
Russian Federation
e-mail: mestlm@mail.ru

2.1 Introduction

The morphological framework is very wide theoretical platform for creation of mid-level image analysis tools for specialized computer vision applications. It utilizes the structural image modeling and is useful for some image filtering, segmentation and comparison problems. The foundation of Mathematical Morphology (MM) by Serra and Matheron was in 1960 [1], and this original version of MM with structuring elements, erosion/dilation operators, and monotonous opening/closing filters is still the most well-known version of MM until nowadays. However, the current morphological framework contains more ideas and tools than the initial MM. Some of them are just unknown for computer vision developers and engineers. The purpose of this chapter is to provide a brief sketch of some novel morphological techniques useful for different practical applications. The chapter contains the following issues:

- Basics of mathematical morphology.
- Skeleton-based continuous binary morphology.
- Morphological pattern spectrum: concepts and computation.
- Morphological image analysis (Pyt'ev morphology).
- Projective morphologies, morphological segmentation, and complexity analysis.

The MM is the most well-known morphological technique based on a set theory and (later) a lattice theory. The idempotent operators (morphological filters or projectors) are introduced using concept of figure filling by structuring elements. In other version, the morphological filters are based on merging of grayscale image connected regions (flat zones). A brief description of basic MM notions and concepts is required for understanding of following techniques.

The continuous binary morphology is a skeleton-based approach for description and analysis of figure shapes proposed and developed by Mestetskiy. It is based on a computational geometry and provides very fast tool for real-time computation of continuous figure skeletons using approximation of 2D binary image by region border polygons and calculation of Voronoi diagram to segment these polygons. A skeletal representation of the figure is formed as a skeleton graph, and the radial function is determined in skeleton points. The computational efficiency of such approach is based on the fact that skeleton-based continuous binary morphology uses the finite and relatively small number of analytical structuring elements for representation of binary image shape. Each analytical structuring element is connected with one edge of continuous skeleton.

A morphological spectrum is a multi-scale morphological shape description and analysis tool based on granulometry—a set of filters with different grades. Each of filters provides the details of certain size and shape to pass. The original “Pattern spectrum” proposed by Maragos is based on the Serra MM filters and describes the distribution of local figure thickness. Many modifications and generalizations of this idea are known and utilized now. In this chapter, the fast algorithm for pattern

spectrum calculation using the continuous binary skeletons is described. Such implementation allows to apply the morphological spectra in the real-time machine vision systems.

The Morphological Image Analysis (MIA) proposed by Pyt'ev is well-known in Russia since 1970. It is based on geometrical and algebraic reasoning. In the framework of Pyt'ev morphology, images are considered as piecewise-constant 2D functions. The tessellation of image frame by a set of the non-intersected connected regions with constant intensities determines the “shape” of the image. From mathematical point of view, any shape is a hyperplane in a linear space of images. The crucial idea of this approach is the projection of one image onto the shape of other image. Here a morphological image comparison is performed using the normalized morphological correlation coefficients. The morphological change detection is performed by a comparison of an image and its projection to the reference image. Such morphological tools are invariant relative to transforms of image intensity and stable relative to noise. In this chapter, a morphological shape matching technique is described that generalizes a morphological approach to shape-to-shape comparison.

A projective morphology is a generalized framework based on the Serra mathematical morphology, the Pavel shape theory, and the Pyt'ev morphological analysis. It combines ideas of these morphological approaches and allows to construct some new morphological systems and operators based on different image decompositions and transforms and/or criteria (energy functions). The criterion-based projective morphological filters are implemented using numeric optimization techniques (linear programming, dynamic programming, graph cutting, and so on). The use of morphological shape complexity as a criterion for shape regularization provides tools for shape complexity analysis those are more general than tools based on the MM granulometry concept. In particular, the definitions of the morphological filters and the morphological spectra by complexity are given.

Thus, some original and modern morphological concepts and tools are presented in this chapter as well as required amount of morphological basics. From one hand, this material allows to learn of modern morphology techniques without any previous background in the MM. From the other hand, some tools and techniques those are applicable for real-time technical vision systems, especially for vision systems of moving vehicles and other controlled real-time technical devices with video cameras or several imaging sensors, are selected and presented.

The chapter is organized as follows. The basics of mathematical morphology are discussed in Sect. 2.2. The skeleton-based continuous binary morphology is described in Sect. 2.3. The concept and computation of morphological spectrum are represented in Sect. 2.4. The morphological image analysis (Pyt'ev morphology) is given in Sect. 2.5. Section 2.6 describes the projective morphologies, a morphological segmentation and a complexity analysis. Conclusion is situated in Sect. 2.7.

2.2 Basics of Mathematical Morphology

The MM is a well-known theoretical framework for image processing and shape analysis. It was originally developed for binary image processing, and classically stated in the set-theoretical terms. Then the MM was extended to grayscale images, color images, graphs, among others. At present, the description of the MM in terms of complete lattices is the widest MM theoretical formalism.

The MM was originally developed by Serra [1] in 1964 and Matheron [2] in 1975. In 1960–1970, the set of popular MM operators was proposed including Hit-or-miss transform, dilation, erosion, opening, closing, granulometry, thinning, skeletonization, ultimate erosion, etc. In 1970–1980, some novel MM operators like morphological gradients, top-hat transform, and the watershed were proposed. In 1986, the MM generalization based on complete lattices was proposed by Serra. In 1990–2000, some further theoretical advancement was developed including the concepts of connection and leveling.

The basic MM concepts and operations in order to explore the interconnections between well-known morphological tools and some novel morphological concepts and ideas are briefly introduced in Sect. 2.2.1. A binary morphology and a grayscale mathematical morphology based on structuring elements are introduced in Sects. 2.2.2 and 2.2.3, respectively. The mathematical morphology as a lattice-theoretic scheme is discussed in Sect. 2.2.4. The novel morphological concept based on connected filters is given in Sect. 2.2.5. A building of morphological skeleton is presented in Sect. 2.2.6.

2.2.1 Mathematical Morphology as a Set-Theoretic Scheme

In a set-theoretic terms [1] the MM operations are defined for any Euclidean space E^N equipped by the set-theoretic inclusion (\subset), union (\cup), and intersection (\cap). Any operator (transform) of this space $\Psi: E^N \rightarrow E^N$ is called:

- The increasing, if it preserves the inclusion $(X \subset Y) \Rightarrow (\Psi(X) \subset \Psi(Y))$, $X, Y \subset E^N$.
- The dilation, if it preserves the union $\Psi(\cup X_i) = \cup \Psi(X_i)$, $\forall X_i \subset E^N$.
- The erosion, if it preserves the intersection $\Psi(\cap X_i) = \cap (\Psi(X_i))$, $\forall X_i \subset E^N$.
- The extensive, if $\Psi(X) \supseteq X$, and anti-extensive, if $\Psi(X) \subseteq X$.
- The idempotent (or algebraic projector), if $(\Psi(\Psi(X))) = \Psi(X)$.

All inclusion-preserving operators are called the morphological operators. Well-known Matheron theorem states that any morphological operator can be represented as a union of erosions or as an intersection of dilations. Due to this theorem, the erosion and the dilation are called the basic morphological operators.

The idempotent morphological operators are called the morphological filters:

- The anti-extensive morphological filter is called the opening.
- The extensive morphological filter is called the closing.

Let us consider the original implementation of these terms and notions.

2.2.2 Binary Mathematical Morphology Based on Structuring Elements

The classic implementation of the formal scheme applying to binary image processing is given in [1]. It is called the binary mathematical morphology. In the framework of this MM, a binary image is considered as a set of non-zero points of the plane $P = R^2$.

Let us define the translation of the set $X \subset P$ by the vector $z \in P$ as the transformation $X_z = \{y | y = x + z, x \in X\}$, where the points of the plane are summed as vectors (coordinates are added component-wise). Let $X, B \subset P$, where $b \in B$ is a Structuring Element (SE). The operation represented by Eq. 2.1 is called the Minkowski addition.

$$X \oplus B = \{x + b | x \in X, b \in B\} = \cup \{B_x | x \in X\} = \cup \{X_b | b \in B\} \quad (2.1)$$

The operation provided by Eq. 2.2 is called the Minkowski subtraction.

$$X \ominus B = \{z \in P | B_z \subseteq X\} \quad (2.2)$$

In the framework of MM these operations (Eqs. 2.1–2.2) are called the dilatation and the erosion of an image X with structuring element B . The dilatation and the erosion are the basic MM operations (see Fig. 2.1). If a structuring element B has a central symmetry relative to the origin of P , then the erosion of binary image corresponds to dilation of figure background (set-theoretic completion) and vice versa (Eq. 2.3).

$$X \ominus B = (X^C \oplus B)^C, X \oplus B = (X^C \ominus B)^C \quad (2.3)$$

The combined operation “dilation after erosion” is called the opening of X by B (Eq. 2.4).

$$X \circ B = (X \ominus B) \oplus B \quad (2.4)$$

It has a clear geometrical meaning—the union of all structuring elements of shape B completely included in figure X : be the following expression:

$$X \circ B = \{B_z | B_z \subseteq X\}.$$

The combined operation “erosion after dilation” is called closing of X by B (Eq. 2.5).

$$X \bullet B = (X \oplus B) \ominus B \quad (2.5)$$

If a structuring element B has a central symmetry relative to the origin of P , then the opening of binary image corresponds to closing of figure background and vice versa as it shown in Eq. 2.6.

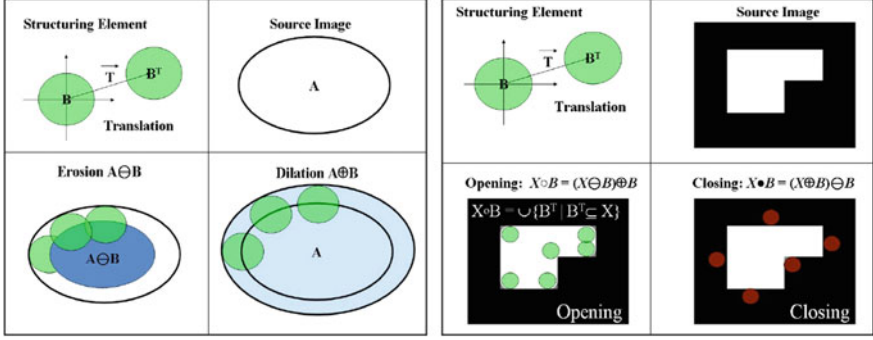


Fig. 2.1 Basic operators and filters of binary MM based on SE

$$X \circ B = (X^C \bullet B)^C, X \bullet B = (X^C \circ B)^C \quad (2.6)$$

If a structuring element B is fixed, then such opening and closing operators are idempotent (projectors) and inclusion-preserving. These operators are called the morphological filters of binary images based on the SEs.

These basic operations and filters of MM were proposed for providing the mathematically founded tools for solution of different practical shape analysis problems. For example, the task for detail extraction of figure based on the expected size and shape can be solved in a way demonstrated in Fig. 2.2.

2.2.3 Grayscale Mathematical Morphology Based on Structuring Elements

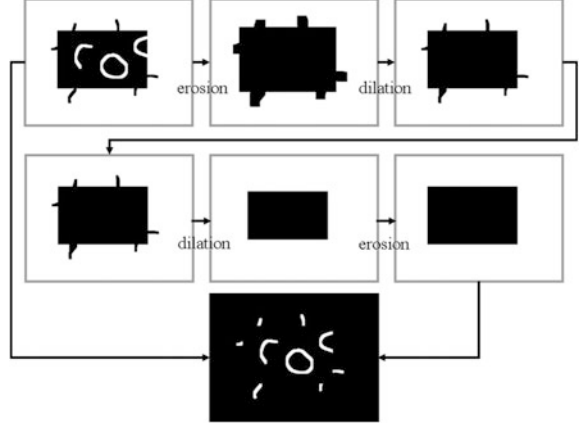
In the framework of grayscale morphology [3–6] the image $f(x, y)$ and a grayscale structuring element $k(u, v)$ are usually represented as the nonnegative two-dimensional functions determined on the plane $P = R^2$ or some square frame $F \subseteq P$. In the simplest way, the grayscale erosion and the grayscale dilation can be determined by Eqs. 2.7–2.8, respectively.

$$f(x, y) \oplus k(u, v) = \max_{(u, v)} \{f(x - u, y - v) + k(u, v)\} \quad (2.7)$$

$$f(x, y) \ominus k(u, v) = \min_{(u, v)} \{f(x + u, y + v) - k(u, v)\} \quad (2.8)$$

The grayscale morphological filters—grayscale opening and grayscale closing are defined as the combinations of grayscale erosion and grayscale dilation provided by Eqs. 2.9–2.10.

Fig. 2.2 The detail extraction using basic morphological operations



$$f \circ k = (f \ominus k) \oplus k, \quad (2.9)$$

$$f \bullet k = (f \oplus k) \ominus k \quad (2.10)$$

The following systematic formulation of grayscale morphology can be given in terms of “image umbra” [3]. Let the set of image f values in frame F be denoted as E . Then umbra of f is a set of 3D points $U(f) \subset F \times E$ lying “under the f ”:

$$U(f) = \{(x, y) \in F \times E | y \leq f(x)\}.$$

The top surface of the set $A \subseteq F \times E$ is a set $T(A): F \rightarrow E$ defined as follows:

$$T[A](x) = \max\{y | (x, y) \in A\}.$$

Based on these notions, one can define the grayscale morphological operations in usual set-theoretic way as described above binary MM operators, but for 3D $(F \times E)$ space point sets. Let $F, K \subseteq E^2, f: F \rightarrow E, k: K \rightarrow E$. Then

- The dilation of f by k SE is $f \oplus k = T[U(f) \oplus U(k)]$.
- The erosion of f by k SE is $f \ominus k = T[U(f) \ominus U(k)]$.

These definitions preserve the set-theoretic background, but in computational sense they are equivalent to previous ones given in terms of min and max operations on pixels of grayscale images.

Another useful way for definition and computation of grayscale morphological operators is based on the notion of grayscale image level sets. This approach was proposed in [7]. For simplicity, let us consider the case of “flat” structuring element with two levels of intensity $k(u, v) \in \{0, -\infty\}$ that corresponds to binary SE $b(u, v) = \{(u, v) | k(u, v) = 0\}$, but for general case of grayscale SE such construction can be defined too.

Let the level image or a slice of grayscale image $f(x, y)$ at intensity level l be a binary image $f_l(x, y) = \{1: f(x, y) \geq l; 0: f(x, y) < l\}$. As it was proved in [7], in the case of “flat” SE all operators of Serra grayscale morphology can be represented as a combination of corresponding binary morphological operators applied to each level of level set as it shown in Eqs. 2.11–2.14.

$$f(x, y) \oplus k(u, v) = \max_{l \in E} \{l \times (f_l(x, y) \oplus b(u, v))\} \quad (2.11)$$

$$f(x, y) \ominus k(u, v) = \max_{l \in E} \{l \times (f_l(x, y) \ominus b(u, v))\} \quad (2.12)$$

$$f(x, y) \circ k(u, v) = \max_{l \in E} \{l \times (f_l(x, y) \circ b(u, v))\} \quad (2.13)$$

$$f(x, y) \bullet k(u, v) = \max_{l \in E} \{l \times (f_l(x, y) \bullet b(u, v))\} \quad (2.14)$$

If a digital image has a fixed and relatively small number of discrete gray levels ($E = 0, \dots, N - 1$), then this approach based on level sets provides the computationally efficient implementation of grayscale morphological operators. Figure 2.3 demonstrates the grayscale morphological operations and morphological detail extraction via corresponding background normalization (difference of source image and morphological filter).

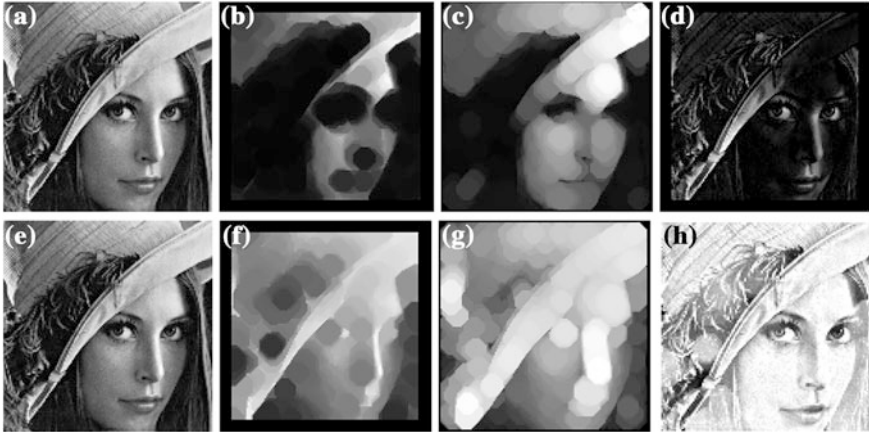


Fig. 2.3 An example of grayscale morphological operators: **a** the source image, **b** the erosion, **c** the opening, **d** the background normalization by the opening (bright details are extracted), **e** the dilation, **f** the connected closing, **g** the background normalization by the closing (dark details are extracted)

2.2.4 Mathematical Morphology as a Lattice-Theoretic Scheme

A complete lattice [8] (L, \leq) is a set L with partial order relation (\leq) such that any subset of this set have the least element (infimum symbolized by \wedge) and the greatest element (supremum symbolized by \vee) with respect to this relation. The least element of lattice is denoted as \emptyset . The supremum of lattice U is called the “universe” of this lattice. Let us note that any pair of elements should have the infimum and supremum. For example, if lattice L is a set of subsets of some set S and ordering relation (\leq) is a set-theoretic inclusion (\subseteq) , then for any $A, B \in S$ (Eq. 2.15).

$$A \wedge B = A \cap B \quad A \vee B = A \cup B \quad (2.15)$$

Let $L = (\{X_i\}, \leq)$. The dilation is an operator $\delta: L \rightarrow L$ and the erosion is an operator $\varepsilon: L \rightarrow L$ [3] provided by Eqs. 2.16–2.17, respectively [9].

$$\bigvee_i \delta(X_i) = \delta(\bigvee_i X_i) \quad \delta(\emptyset) = \emptyset \quad (2.16)$$

$$\bigwedge_i \varepsilon(X_i) = \varepsilon(\bigwedge_i X_i) \quad \varepsilon(U) = U \quad (2.17)$$

For every dilation δ , there is one erosion ε such that

$$X \leq \varepsilon(Y) \Leftrightarrow \delta(X) \leq Y \quad \text{for all } X, Y \in L$$

and vice versa: every erosion have the dilation satisfying the above condition. Moreover, if δ and ε satisfy this condition, then they must be the dilation and erosion. Such pairs of connected operations are called the adjunctions. For every adjunction (ε, δ) , the morphological opening and the morphological closing are defined by Eqs. 2.18–2.19, respectively.

$$\gamma: L \rightarrow L: \gamma = \delta \varepsilon \quad (2.18)$$

$$\phi: L \rightarrow L: \phi = \varepsilon \delta \quad (2.19)$$

2.2.5 Morphologies Based on Connected Filters

The connected filters are the connectivity preserving morphological filters [8, 10, 11]. The image domain (frame) can be partitioned into the disjoint sets based on connected components (in the binary case) or the connected zones of constant grey/color levels (in the greyscale/color case). A connected filter works by merging the disjoint sets in the partition and assigning new grey levels or colors to them. This means that no new edges are introduced by the connected filters. A connected

filtering operates with image regions rather than pixels. Obviously, such filtering depends on a definition of connectivity (8 or 4 neighbors for pixel).

The grayscale connected operators act by merging of flat zones (regions of constant intensity). A partition is a set of nonoverlapping, nonvoid regions that fills the entire space. Let \mathbf{P} is the partition of the frame, $P(n)$ is a region of \mathbf{P} that contains pixel n . A partial order relationship of complexity among partitions can be defined as follows: \mathbf{P}_1 is finer than \mathbf{P}_2 ($\mathbf{P}_1 \subseteq \mathbf{P}_2$), if $\forall n: P_1(n) \subseteq P_2(n)$.

The set of flat zones of image f is a partition of space P_f . A grayscale operator ψ is connected, if the partition of flat zones of its input f is always finer than the partition of flat zones of its output $\psi(f)$, that is $P_f \subseteq P_{\psi(f)}$, $\forall f$.

The connected filters bridge the gap between filtering and segmentation. Figure 2.4 demonstrates an image and its filtered version with corresponding partition. This example illustrates the simplification of the image shape by the connected filter.

There are three types of connected filters:

- The filters by reconstruction perform the reconstruction of connected regions (flat zones) after their processing by some ant-extensive operator, for example, some SE erosion.
- The area filters delete regions (flat zones) with area lower than some threshold.
- The attribute filters delete regions (flat zones) with some region attributes (area, perimeter, diameter, inertia moment, etc.) non-satisfying the predefined rules (for example, lower or higher than some threshold). The area filters and filters by reconstruction are the particular cases of attribute filters.

The connected and the SE based filters complement each other in the shape analysis applications providing different tools for morphological image transformation and object selection. Such transformation means the modification of image connectivity and shape. The selection presumes an elimination or an extraction (using the background normalization scheme) of image elements with given shape, size, and contrast sign. These properties of filters are contradictive, and should be separated. Connected filters provide the solution of this problem. An example of morphological corner detection via combination of opening and connected opening is shown in Fig. 2.5. Figure 2.6 provides an example of grayscale connected morphological filters—opening and closing by reconstruction [12].

2.2.6 Morphological Skeleton

A morphological skeleton is a compact description of 2D figure shape that can be obtained by some sequence of morphological operations and provides the possibility for reconstruction of described shape using some other sequence of morphological operations. The morphological formula for the skeleton of a continuous binary image was proposed in [1, 13]. For discrete case this formula is implemented as follows. Let $\{nB\}$, $n = 0, 1, \dots$, be a sequence of shapes based on some structuring element B , $nB = B \oplus \dots \oplus B$ (n times), and $OB = \{o\}$, where o is the



Fig. 2.4 The simplification of image by the connected filter: **a** the source grayscale image, **b** the image filtered by connected version, **c** corresponding frame partition

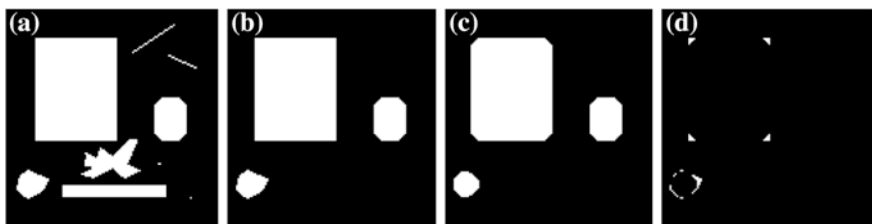


Fig. 2.5 An example of morphological corner detection: **a** the source image, **b** the result of connected opening by SE and reconstruction, **c** the result of SE opening, **d** the result of the corner extraction operator (background normalization—difference between connected opening and SE opening)

origin of 2D image plane, n is a size of the structuring element nB . A discrete skeleton $S(X)$ of a discrete binary image $X \subset \mathbb{Z}^2$ (Fig. 2.7a, b) is the union of the skeleton subsets $\{S_n(X)\}$, $n = 0, 1, \dots, N$ provided by Eq. 2.20.

$$S_n(X) = (X \oplus nB) - (X \oplus nB) \circ B \quad (2.20)$$

The reconstruction of original shape X from the skeleton is performed by Eq. 2.21 while the partial reconstruction corresponds to the opening of original shape is represented by Eq. 2.22.

$$X = \bigcup_n (S_n(X) \oplus nB) \quad (2.21)$$

$$\bigcup_{n \geq m} (S_n(X) \oplus nB) = X \circ mB \quad (2.22)$$

In the next Sect. 2.3, another approach for definition and computation of continuous skeletons based on concept of medial axes as a set of centers of maximal inscribed balls (discs) will be considered.

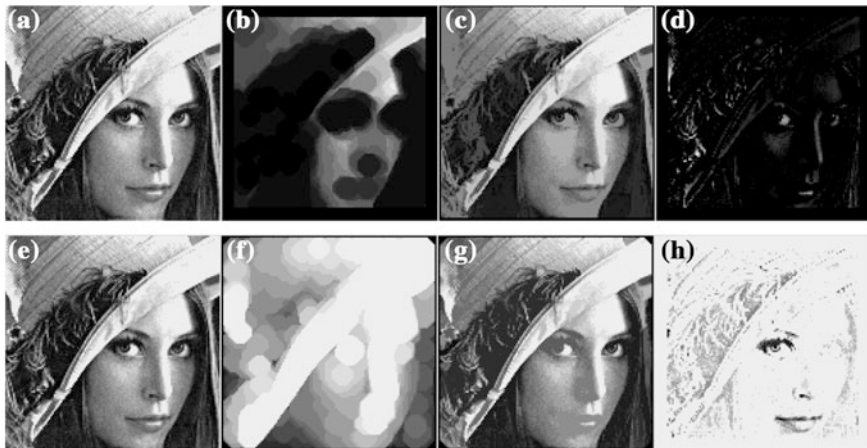


Fig. 2.6 An example of grayscale connected morphology operators: **a** the source image, **b** the erosion, **c** the connected opening, **d** the background normalization by the connected opening, **e** the dilation, **f** the connected closing, **g** the background normalization by the connected closing

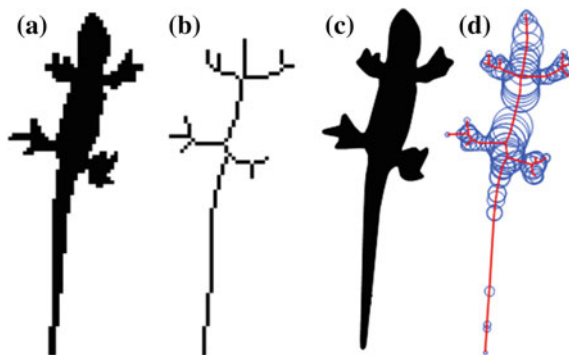


Fig. 2.7 The discrete approach of skeleton building: **a** the discrete binary image, **b** the discrete skeleton, **c** the continuous binary image, **d** the continuous skeleton and inscribed circles

2.3 Skeleton-Based Continuous Binary Morphology

This section is devoted to skeleton-based continuous binary morphology. The main concepts for the skeleton of binary images are presented in Sect. 2.3.1. The continuous representation of raster image boundary is discussed in Sect. 2.3.2. A polygonal figure skeleton based on the Delaunay graph is described in Sect. 2.3.3. Section 2.3.4 provides the novel skeleton-based continuous binary morphologies.

2.3.1 *Skeleton of Binary Image Versus Binary Image of Skeleton*

The skeleton (or medial axis representation) is a powerful and widely used tool for image shape analysis [14]. The concept of the skeleton (the middle set of points) was introduced and investigated by Blum [15]. The skeleton of a closed region in Euclidean plane is a locus of centers of maximum empty circles in this region. The circle is considered to be empty, if all its internal points are internal points of the region. One can formulate two approaches to extend the concept of the skeleton to discrete images.

The first approach, which is the most popular, will be called discrete. It consists in a morphological transformation of the original image (Fig. 2.7a) and a construction of a new image (Fig. 2.7b), which can be regarded as a skeleton. In this new bitmap, a medial axis is represented by discrete lines one pixel width. One can say that the resulting image is a digital image of the skeleton. The discrete approach is implemented in different ways: based on distance maps, thinning, Voronoi diagrams of boundary points [16, 17]. The main advantage of the discrete approach is the simplicity of the algorithm and a graphic visualization of the skeleton in the source raster format (Fig. 2.7a, b).

Another approach, which is called continuous, is based on the approximation of a discrete object by the geometrical figure in terms of a continuous geometry (Fig. 2.7c) and the construction of the skeleton for this figure (Fig. 2.7d). The resulting skeleton is considered as a continuous skeleton of discrete objects.

A continuous approach has its advantages. The main advantage of the approach is the continuous medial representation of the object's shape [17] as a geometrical graph with a radial function, which determines the width of the object. The radial function sets at each point of the geometrical graph radius of the inscribed circle are centered at this point. A continuous medial representation allows the use of graph theory and computational geometry algorithms for image shape analysis and recognition.

A comparative analysis shows the advantages of continuous skeleton compared to discrete one. These advantages are mathematical rigor, information content, and computational efficiency. This section is based on the studies described in papers and books [18–23] and provides the full implementation of the continuous approach to the skeleton construction for binary raster images of any complexity. Here an original method for continuous skeleton representation as a planar graph, whose edges are segments of straight lines and quadratic parabolas, is represented. The concept of continuous skeleton for raster binary image is developed to use the correct and elegant model of Voronoi diagram of line segments and polygonal figures to obtain the skeleton of a discrete object.

The proposed idea consists of three parts (Fig. 2.8):

- The approximation of binary image (Fig. 2.8a) by a polygonal figure (Fig. 2.8b).
- The computation of Voronoi diagram of obtained set of figures by methods of computational geometry (Fig. 2.8c).

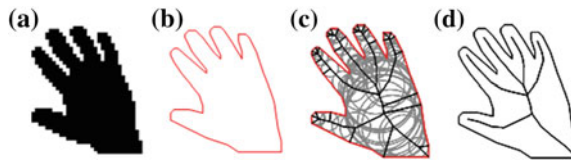


Fig. 2.8 The continuous approach: **a** the source binary image, **b** the polygonal approximation, **c** the medial representation of the polygon, **d** the resultant skeleton after pruning

- The obtaining of the skeleton from the Voronoi diagram in a convenient format for further analysis (Fig. 2.8d).

The choice of a polygonal figure for the approximation is explained by the fact that the skeleton of a polygonal figure is a fairly simple structure and can be obtained from the Voronoi diagram of this figure. The implementation of this approach required solving of several computational problems addressed below.

2.3.2 Continuous Representation of Raster Image Boundary

Let the object points of binary image be black, and the background points be white. Let us define an adjacency structure on a set of pixels as follows. For a black pair of pixels, the neighborhood of 8-adjacency and, for a white pair and black-white pair, the neighborhood of 4-adjacency are defined. A set of one-colored pixels is called connected, if, for each pair of pixels into it, there is a path from one pixel to another consisting of sequentially neighboring pixels of the same color. The maximal connected set of pixels of one color is called a connected component. The discrete figures are the connected black-colored components.

Let us call a pair of 4-adjacent black-white points as a boundary pair, and a segment connecting these points as a boundary segment. Two components, to which points of a boundary pair belong, are called adjacent, and the boundary pair is called a dividing for these components. A set of all dividing boundary pairs for two adjacent components let us call a boundary corridor. Each discrete figure defines one or more boundary corridors.

There is a minimal length path among all closed paths lying in a boundary corridor. This path is a closed polyline called a separating Minimal Perimeter Polygon (MPP). The set of all MPP of a discrete figure defines a polygonal figure (polygon with polygonal holes). Thus, we have defined the polygonal figures with minimal perimeters, which approximate the discrete figures in a binary image. The set of approximating polygonal figures exists and unique for any binary image.

The line scanning of image rows is used for tracing of all contours. Such tracing consists of detection the first boundary pair and sequential finding the next boundary pairs until the returning to start position. A process ends, when a line scanning of image rows is completed, and all contours are extracted.

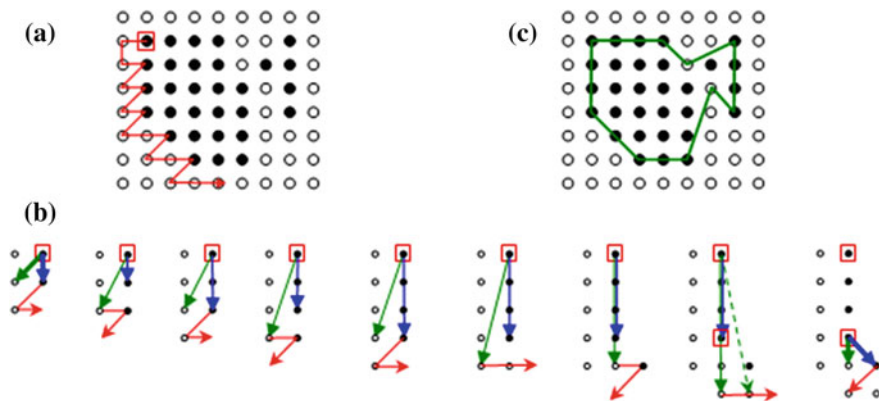


Fig. 2.9 Detection of next corner point for the minimal perimeter polygon: **a** the initial corner point, **b** the obtaining of next corner point by sequential steps for the correction of the coverage sector, **c** the minimal perimeter polygon

The sequence of contour points forms an ordered list called a tracing track. All vertices of MPP are points of a tracing track. Let us call such point a corner. Figure 2.9 illustrates the process of the MPP constructing. Figure 2.9a shows the first corner point and a part of the tracing track. Figure 2.9b presents the sequential steps of coverage sector correction from starting position (left image) until the next corner is obtained (right image). Figure 2.9c shows the final obtained MPP.

2.3.3 Polygonal Figure Skeleton

The Voronoi diagram and the Delaunay graph of polygonal figure. Let $P \in R^2$ be a multiple-connected polygonal domain and $S(P)$ be a set of all sites of P ($S(P)$ consists of all vertices and sides of P called vertex-sites and segment-sites, respectively). The medial axis $M(P)$ is a subset of Voronoi diagram $VD(P)$ of the site set of P . This is the feature most algorithms computing medial axis of a polygonal figure rely on.

The concept of the Voronoi diagram for line segments is commonly used for a skeleton construction of a polygonal figure [24, 25]. The polygonal figure boundary is a union of linear segments and vertices, which are considered as the Voronoi sites. The Voronoi diagram of these sites is generated, and the skeleton is extracted as a subset of the diagram. The skeleton of a polygonal figure with n sides can be obtained from the Voronoi diagram taking $O(n)$ time. By-turn, there are known the effective $O(n \log n)$ algorithms to construct the Voronoi diagram for the general set of linear segments [26, 27] as well as for the sides of a simple polygon [28] or multiple-connected polygonal figures [22].

A polygonal figure skeleton looks like a planar graph with edges consisting of line segments and parabolas [29, 30]. Skeleton vertices are convex vertices of a polygonal figure (one degree vertices) and also points—centers of inscribed circles tangent to figure boundary in three or more points (three and more degree vertices). The radial function is defined in each skeleton point as the radius of inscribed circle centered in this point. It is especially necessary to note that the polygonal figure skeleton always exists and is unique.

The construction of skeleton based on the Delaunay graph. The main idea of the algorithm is based on constructing the Delaunay graph of figure sites and an adjacency tree of figure boundary contours (Fig. 2.10).

Let P be a multiple-connected polygonal domain. Two sites of P are adjacent, if they are adjoining to each other (vertex-site and segment-site of a common side) or there exists a disk inscribed in P and touching both sites (in other words, if their Voronoi cells have non-empty intersection). The Delaunay graph $DG(P)$ of P is a graph (S, E_S) , where S is a set of sites of P and $E_S \subseteq S \times S$ contains all pairs of adjacent sites from S . Similarly, the Delaunay graph of a subset S' of S is defined as a graph $(S', E_{S'})$, where $S' \subseteq S$ and $E_{S'} \subseteq S' \times S'$ contains all pairs of adjacent sites from S' .

The Delaunay graph of P is a dual structure for the Voronoi diagram of P . The duality of $DG(P)$ and $VD(P)$ is that there a bijection between their structure elements exists: every $VD(P)$ vertex with its incident edges and incident faces is assigned to $DG(P)$ face with its incident edges and incident vertices. Given $DG(P)$ constructed, the $VD(P)$ can be obtained in $O(n)$ time.

The algorithm to transform the Delaunay graph to the corresponding Voronoi diagram is described in [31]. Actually, under the non-degeneracy assumption that no point in the plane is equidistant to more than three sites of P , the Delaunay graph is the triangulation of a set of the sites of P (possibly, with non-straight edges).

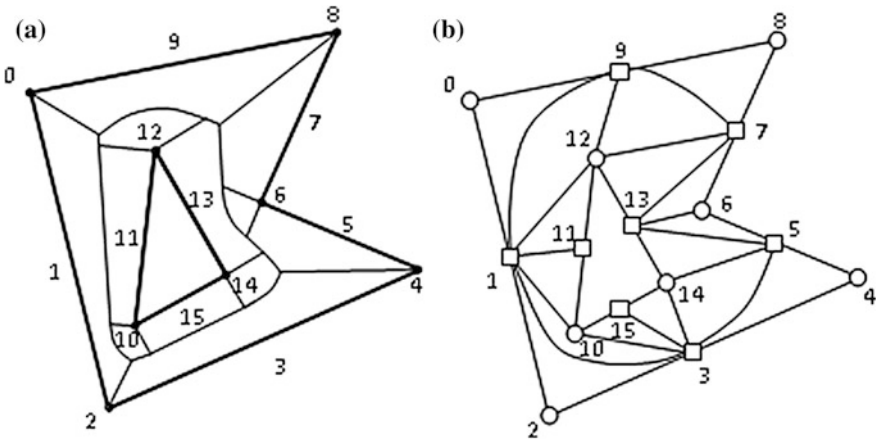


Fig. 2.10 A polygonal domain site set: **a** the Voronoi diagram, **b** the Delaunay graph (circles denote vertex-sites and squares denote segment-sites)

The algorithm to compute the Delaunay graph of a simple polygon involves the steps mentioned below:

1. The generating initial elementary chains of sites and constructing their Delaunay graphs.
2. The iterative pairwise merge of Delaunay graphs of chains. At each iteration the following operations are performed as follows:
 - The clearing Delaunay graphs in every pair so that the Delaunay condition is satisfied for every edge relative to the union of sites from both graphs in the pair. At this stage some edges can be eliminated in every pair of the Delaunay graphs.
 - The “sewing” of the Delaunay graphs in every pair so that the Delaunay condition is satisfied for every new inserted edge relative to the union of sites from both graphs in the pair. At this stage, every pair of the Delaunay graphs is “sewed” and new Delaunay graphs are formed.

The computational complexity of the algorithm is $O(n \log n)$. This algorithm is similar to one proposed in [29] for merging Delaunay triangulations.

A skeleton of multiple-connected polygonal figure. Fast algorithms for constructing skeleton of simple polygon with n vertices through Voronoi diagram have a computational complexity $O(n \log n)$ in the worst case [28]. The known generalizations to the case of a polygonal figure with holes [32–34] have computational complexity $O(kn + n \log n)$, where k is a quantity of polygonal holes, n is a general number of vertices. Such computational complexity leads to high costs in time. For example, in the problem of construction of an external skeleton for segmentation of the text document image [18] values k and n have an order 10^3 and 10^5 , respectively. At the same time, the efficient algorithms for Voronoi diagram construction of linear segment set [26, 27] do not use specific features of segment set of polygonal figure boundary owing to their universality. In particular, these algorithms build Voronoi partitioning not only inside, but also outside of a polygonal figure, and this is a superfluous work.

This solution is based on concept definition for adjacency of polygonal figure boundary contours and on construction of so-called adjacency tree of these contours. Two boundary polygons are adjacent, if the circle inscribed into a figure and contacted both of these polygons exists. The given relation of contour adjacency defines a graph of contour adjacency. It is obvious that this graph is connected. Each spanning set of it (the minimal connected spanning subgraph) is a tree. Such tree is called a boundary adjacency tree of a polygonal figure. The boundary adjacency tree gives the chance to reduce a problem of a polygonal figure skeletonization to a problem of a simple polygon skeletonization. Let us transform chains of side of polygons by “cutting-in” them into one another. As a result the polygonal figure conditionally transforms to “polygon”. In details, this process was described in [18]. The $O(n \log n)$ sweepline algorithm for finding a boundary adjacency tree and a figure skeleton construction on its basis is described *ibidem*.

A skeletal base of polygonal figure. Small irregularities in figure boundary lead to occurrence of skeleton branches unessential for analysis of image form. A problem of skeleton regularization consists in removing these branches and leaving only fundamental part of a skeleton, which characterizes properties of the form. This fundamental part looks like a skeleton subgraph. Let us call it a skeletal base. A transformation of a skeleton to a skeletal base consists in removing of unessential vertices and edges. This process is called a “pruning”.

Let C be a polygonal figure with the boundary ∂C , the skeleton S , and the skeleton radial function $\rho(s)$, $s \in S$. The skeleton is a planar graph $S = (P, E)$ with the set of vertices P and edges E . A skeleton vertex with one incident edge is a terminal, and with two or more edges is an internal. An edge incident to terminal vertex is also called terminal. An edge incident to two internal vertices is called linking. The linking edges can be included in one or more cycles, and in this case they are called cyclic.

A pruning is an iterative removal of “unessential” terminal vertices and skeleton edges. Essential edges remain in a skeletal base. A pruning preserves a skeleton connectivity and all cycles. Let $S' = (P', E')$ be some connected subgraph of skeleton $S = (P, E)$ such that $P' \subseteq P$, $E' \subseteq E$, and there are no cyclic edges of skeleton S among edges from the set $E \setminus E'$ (Fig. 2.11). Such graph S' is called a truncated subgraph of S . Consider the set of points formed by union of all inscribed circles centered in points of truncated subgraph S' , which radiuses are equal $\rho(s)$, $s \in S'$. This set of points forms the closed region, which is called a silhouette of subgraph S' . The important property of a truncated subgraph silhouette is the topological equivalence to figure C . In particular, it is a connected set.

A skeletal base of figure C is the minimal truncated subgraph S' of its skeleton S with ε -silhouette $V_{S'}$ satisfying a condition $H(C, V_{S'}) \leq \varepsilon$, where $\varepsilon > 0$ is regularizing parameter and $H(C, V_{S'})$ is the Hausdorff distance between a figure C and a silhouette $V_{S'}$. For each value of parameter ε the skeletal base always exists and is unique as well as its ε -silhouette. One can call the skeletal base as a continuous skeleton of a discrete figure (Fig. 2.12). A computational complexity of algorithm depends linearly on a number of skeleton vertices, i.e. it is equal $O(n)$ at the worst case, where n is a quantity of polygonal figure vertices.

2.3.4 Skeleton-Based Continuous Binary Morphologies

Let us consider the MM with disk structuring element $D(r)$ of size r . Continuous binary opening requires the infinite number of disks for shape reconstruction

$$P \circ D(r) = \bigcup_{D(r) \subseteq P} D(r).$$

That is why the continuous MM filters are usually out of consideration.

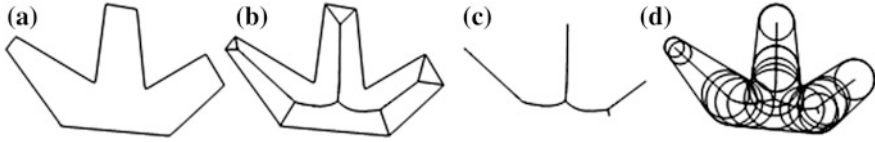


Fig. 2.11 A construction of skeletal subgraph silhouette: **a** the initial image, **b** the skeleton, **c** the truncated subgraph of skeleton, **d** the silhouette of the subgraph

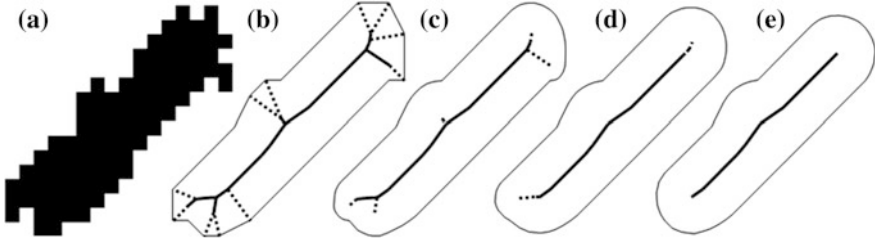


Fig. 2.12 The skeletal base construction: **a** the initial image, **b** the polygonal figure and its skeleton, **c–e** the skeleton subgraphs and their silhouettes

On the other hand, considering the notion of continuous skeleton, Eq. 2.23 for continuous MM opening can be obtained, where $D(p, t)$ is an empty disk of size t with center p , $S(P)$ is a skeleton of figure P .

$$P \circ D(r) = \cup_{p \in S(P)} \{D(p, t) : t \geq r, D(p, t) \subseteq P\} \quad (2.23)$$

If a figure P is polygonal, then its skeleton consists of finite number of line and parabolic segments. This allows representing the figure as a union of finite number of ANalytical struCTure ELEments (anxels) (Fig. 2.13). Let each i th edge of skeleton $S(P)$ is denoted as S_i . The silhouette of S_i (a union of all empty disks centered on S_i) let us call the i th anxel of figure P and denote it as P_i . Thus, an anxel representation of figure P takes the form of Eq. 2.24, where n is a number of skeleton edges.

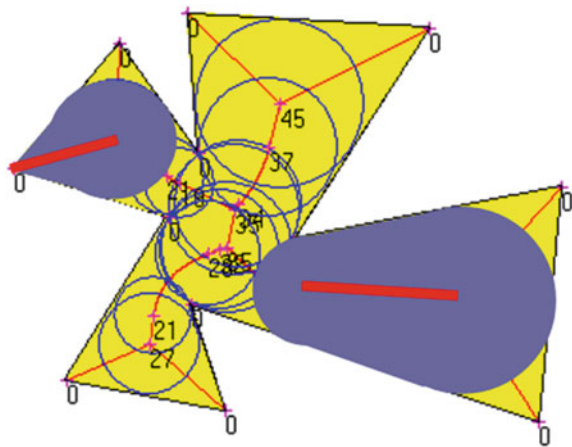
$$P = \cup_{i=1, \dots, n} P_i \quad (2.24)$$

Therefore, the opening of P can be represented by Eq. 2.25.

$$P \circ D(r) = \cup_{i=1, \dots, n} \cup_{p \in S_i} \{D(p, t) : t \geq r, D(p, t) \subseteq P_i\} = \cup_{i=1, \dots, n} P_i \circ D(r) \quad (2.25)$$

The opening of each anxel can be calculated analytically: a silhouette of r -opened anxel P_i will be empty (if all radial function values on S_i are less than r) or bordered by parts of its initial border and possibly parts of circles of size r .

Fig. 2.13 A skeleton of polygonal figure and analytical structure elements (anxels)



Let us note that a mapping of figure P to its ε -silhouette described above also satisfies the properties of morphological filter (opening), and such ε -opening can be described in analogous way using the anxel figure representation as a process of ε -exclusion and ε -cutting of terminal anxels. In both cases of anxel-based morphologies, a corresponding continuous closing is implemented via continuous opening of a figure background. Thus, the anxel representation of polygonal figures allows to define different continuous binary morphologies with different continuous filters based on selection and/or transformation of figure or background anxels.

In the next Sect. 2.4 the applicability of this approach for efficient calculation of morphological pattern spectrum will be demonstrated.

2.4 Morphological Spectrum: Concept and Computation

A morphological spectrum is one of special tools from the reach morphological toolbox. The original Pattern Spectrum (PS) was proposed by Maragos [35] based on the MM filters with SE [1]. It describes the distribution of local figure thickness. Later some modifications and implementations were proposed. All modifications and generalizations of the PS one can refer as the morphological spectra. The morphological spectra are the sensitive and stable descriptors of image shape especially useful for texture analysis, object selection, tuning of morphological filtering and segmentation parameters [11, 36, 37]. However, for many years this morphological tool was not so popular because of its very expensive computational implementation. In this section, let us discuss a computationally efficient approach to morphological spectra calculation based on thickness map concept, continuous skeletal representation [38], and level decomposition of morphological filters [39]. This approach provides a possibility to use the morphological spectra in real-time vision applications.

The pattern spectrum and morphological spectra are discussed in Sect. 2.4.1. The thickness map and morphological spectrum are located in Sect. 2.4.2. Section 2.4.3 contains a calculation of binary morphological spectra based on continuous skeletal representation while as well as a calculation of grayscale morphological spectra is given in Sect. 2.4.4.

2.4.1 Pattern Spectrum and Morphological Spectra

Let B is a figure (compact and convex point set) of the plane P including the origin. Then the figure rB of shape B and size r is defined as follows

$$rB = \{rb = (rx, ry) | b = (x, y) \in B\}, r \geq 0.$$

The morphological PS (PS_X) of figure $X \subseteq P$ with structuring element B [35] is defined by Eqs. 2.26–2.27, where $S(X)$ is an area of figure X . Equations 2.26–2.27 specify the spectrum for positive and negative parts of the r axis, respectively.

$$PS_X(r, B) = -\partial S(X \circ rB) / \partial r \quad r \geq 0 \quad (2.26)$$

$$PS_X(-r, B) = \partial S(X \bullet rB) / \partial r \quad r > 0 \quad (2.27)$$

The Discrete Morphological Pattern Spectrum (DMPS) of X [35] is defined by Eqs. 2.28–2.29, where $r_i = i\Delta r, i \in \mathbb{Z}, \Delta r$ is a sampling step of the scale r .

$$PS_{X,B,\Delta r}(r_i) = -\frac{S(X \circ r_i B) - S(X \circ r_{i+1} B)}{r_i - r_{i+1}} \quad r \geq 0 \quad (2.28)$$

$$PS_{X,B,\Delta r}(r_i) = \frac{S(X \bullet (-r_i B)) - S(X \bullet (-r_{i+1} B))}{r_{i+1} - r_i} \quad r < 0 \quad (2.29)$$

The special test image filled by disks of different size is shown in Fig. 2.14. If $B = D$ is a disk SE, then $S(X \circ rB)$ will be the step function of r with steps at each size of disks presented in the image, and the amplitude of the step is equal to the sum of areas of disks with this size. Hence, positive part of discrete pattern spectrum contains peaks corresponding to these steps with the same amplitude.

As noted in [35], the PS conveys four useful types of information about X . A boundary roughness of X relative B determines peaks in the lower size part of the PS. The long capes or bulky protruding parts in X consisting of patterns rB produce isolated impulses in the positive part of the PS at r scale value. The B-shapeness of X is a maximal degree of rB in X measured by ratio $PS_X(r, B)/S(X)$. The left part of the spectrum (r is negative) demonstrates the significant isolated impulses, if corresponding gulfs or holes are in X .

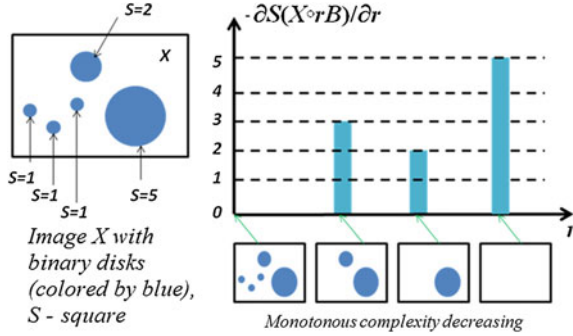


Fig. 2.14 A positive part of morphological spectrum with disk SE and corresponding steps of opening with increasing disk size providing changes in opened figure area

From theoretical point of view, the PS with all its modifications and generalizations (morphological spectra) are based on granulometries—the sets of morphological filters of different grades, each allowing details (grains) of certain size classes to pass. Let $\{\gamma_k\}$, $k = 0, 1, \dots$ be a set opening operators $\forall X \gamma_0(X) = X$, $\gamma_{k+1}(X) \subseteq \gamma_k(X)$. For example, $\gamma_k(X) = X \circ r_k B$. A granulometry function $G_k(X)$ is a cardinality (area, volume, etc.) of the pattern $\gamma_k(X)$: $G_k(X) = |\gamma_k(X)|$. The PS or size distribution of X will be a sequence of differences, produced by sequential subtraction of granulometry function values provided by Eq. 2.30.

$$PS_X(k, \gamma) = G_k(X) - G_{k+1}(X) \quad (2.30)$$

Another generalized scheme was proposed by Matheron in terms of sieving by series of sieves with decreasing the sizes of holes. The filtering of X through k th sieve $\Psi_k(X)$ returns the subset of X sub-elements with sizes not greater than k .

The sieving operators $\{\Psi_k(X)\}$, $k = 0, 1, \dots$ have the following properties:

- The anti-extensive: each sieve reduces the amount of grains, i.e. $\Psi_k(X) \subseteq X$.
- The increasing: a sieving preserves the inclusion, i.e. $X \subseteq Y \Rightarrow \Psi_k(X) \subseteq \Psi_k(Y)$.
- The stable: a passing through two sieves is determined by the smallest hole size, i.e. $\Psi_k \Psi_m(X) = \Psi_m \Psi_k(X) = \Psi_{\max(k,m)}(X)$.

Such sequences of operators are the base of granulometry.

From practical point of view, there are two main classes of morphological spectra: based on filters with SEs and based on the connected filters. The first class contains the original PS [35], the spatial morphological shape-size PS proposed by Wilkinson [40], and some other. The second class includes the size pattern spectra, the shape pattern spectra, the binned 2D shape-size PS [41], and so on.

The morphological spectra based on the SEs are robust and have invariant shape-size descriptors but they are very computationally expensive because they require one opening operation per bin of the spectrum. Therefore, the efforts for improvement of such technique were put to the creation of fast SE filters

computation algorithms [42–50]. The best result was obtained by Urbach and Wilkinson [50]. They have proposed the efficient 2D grayscale morphological transformation with arbitrary “flat” SEs. This algorithm is based on decomposition of SE into “chords”. However, even the use of this fast algorithm provides the SE spectrum computation time about s per image in the best case.

The morphological spectra based on the connected filters may use the attribute openings taking in account both width (thickness) and any other attributes of flat zones. Some of these spectra (with simplest filtering of flat zones by area) even can be implemented for real-time processing. Unfortunately, such spectra do not contain the information about local thickness that characterizes the original PS. Therefore, for real-time implementation the computational approach of the SE morphological spectra calculation, which does not require one opening for each bin, ought to be designed.

2.4.2 Thickness Map and Morphological Spectrum with Disk Structuring Elements

The PS describes the distribution of local figure thickness. This fact points the alternative way for calculation based on the notion of thickness map. Let a rectangular frame K completely contains figure X : $X \subseteq K$. A binary image consists of figure X and its background $X^{C(K)} = K \setminus X$ and described by Eq. 2.31.

$$f_X(x, y) = \begin{cases} 1 & \text{if } p = (x, y) \in X \\ 0 & \text{if } p = (x, y) \in X^{C(K)} \end{cases} \quad (2.31)$$

The thickness map $t_{X,B}(x, y)$ of continuous binary image f_X with structuring element B is a real-valued 2D function defined on the frame K . In this map, all points of the figure have positive values equal to the maximal size of inscribed disk centered in this point. The background values are negative with magnitude equal to the maximal size of disk centered in this point, and they are inscribed to a figure completion. A relation between thickness map and Serra MM filters is provided by Eq. 2.32.

$$X \circ rB = \{(x, y) : t_{X,B}(x, y) \geq r\} \quad X \bullet rB = \{(x, y) : t_{X,B}(x, y) \geq -r\} \quad (2.32)$$

Let us define the function

$$\chi_{X,B}(x, y, r) = \begin{cases} 1 & t_{X,B}(x, y) \geq r \\ 0 & \text{otherwise} \end{cases}$$

and introduce a following measure

$$\mu_{X,B}(r) = \|\chi_{X,B}(x, y, r)\|_{L^1} = \int \int \chi_{X,B}(x, y, r) dx dy$$

$$\mu_{X,B}(r) = \begin{cases} \|X \circ rB\|_{L^1} : r \geq 0 \\ \|X \bullet (-r)B\|_{L^1} : r < 0 \end{cases}$$

Therefore, the PS according to Eqs. 2.26–2.27 is a distribution density function of thickness map determined by Eq. 2.33.

$$PS_{X,B}(r) = -\partial \mu_{X,B}(r) / \partial r \quad (2.33)$$

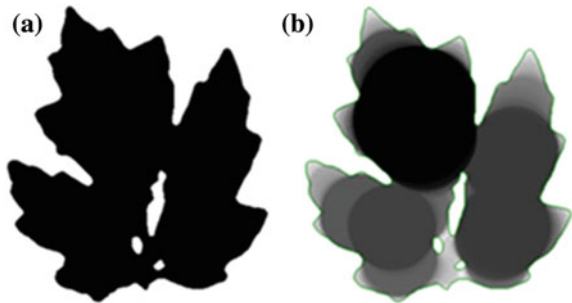
In similar way, one can show that a discrete morphological PS (Eqs. 2.28–2.29) is equal to histogram of discrete thickness map. Let us additionally note that the positive part of the thickness map (Fig. 2.15) and the positive part of the morphological PS remain unchanged, when a figure is shifted or rotated in frame.

Thus, if a thickness map is built, then one opening or closing operation for each bin of the spectrum is not required: just to collect the histogram of a thickness map is needed. However, some computationally efficient algorithm to calculate the thickness map ought to be designed.

2.4.3 Calculation of Binary Morphological Spectra Based on Continuous Skeletal Representation

The crucial idea of fast thickness map computation is derived from the fact that the centers of all empty discs (inscribed in figure and background) belong to the figure's skeleton. Thus, the information required for thickness map computation is already stored in a skeletal representation—skeleton and radial function. In this section, the continuous binary morphology given by Mestetskiy [38] and briefly represented in previous sections will be described. This approach provides the

Fig. 2.15 Example of thickness map: **a** a binary figure X , **b** a positive part of thickness map for a figure X



real-time algorithm for computation of skeletal representation based on the use of generalized Voronoi diagrams [51].

The thickness map forming algorithm is based on the voting of skeleton points into the two-dimensional discrete accumulator array with the same size as binary image to be processed [52–55]. Each continuous skeleton edge is rasterized using the Brezenham algorithm [56], and then each discrete edge point votes for all discrete accumulator cells (pixels) covered by empty disk centered in this point. The purpose of voting is to determine the maximal size (radius) of covering empty disk for each pixel of binary image. The histogram of accumulated maximal thickness values is called the Discrete-Continuous Morphological Pattern Spectrum (DCMPS) [55] due to discrete accumulation based on continuous skeleton. Figure 2.16 demonstrates the binary image of a figure, the positive part of its thickness map, the positive part of DCMPS, and the selected parts of figure with minimal width (local thickness) corresponding to peaks in a spectrum.

The experiments with software implementation of this algorithm have demonstrated the computational time for binary pattern spectrum calculation less than 10 ms for 640×480 binary image on PC configuration CPU Core i5-2320, 3.0 GHz, RAM 2 GB. Therefore, this algorithm can be applied for real-time implementations.

2.4.4 Calculation of Grayscale Morphological Spectra

In the grayscale morphology with image $f(x, y)$ and structuring element $k(u, v)$ the grayscale spectrum PS_f is defined by Eqs. 2.34–2.35 [35], where r is the size of SE $rk(x, y)$ and norm $\|f\|$ is a volume of umbra $U(f)$.

$$PS_f(r, k) = -\partial\|f \circ rk\|/\partial r \quad r \geq 0 \quad (2.34)$$

$$PS_f(-r, k) = \partial\|f \bullet rk\|/\partial r \quad r > 0 \quad (2.35)$$

The use of a level decomposition for the morphological operators allows fast calculation of morphological spectrum for grayscale images and filters with “flat” SEs. Let us consider the discrete N -level two-dimensional function $f(x, y) \in \{0, 1, \dots, N-1\}$ reconstructable from N binary level sets as it is shown in Eq. 2.36.

$$f(x, y) = \sum_{l=0, \dots, N-1} \{f_l(x, y)\} = \max_{l=0, \dots, N-1} \{l \times f_l(x, y)\} \quad (2.36)$$

The “flat” SE has two levels of intensity $k(u, v) \in \{0, -\infty\}$ and corresponds to binary SE $b(u, v) = \{1 \text{ if } k(u, v) = 0, 0 \text{ if } k(u, v) < 0\}$. As shown in [39], the filters of Serra grayscale morphology with “flat” SE may be presented as a combination of corresponding binary MM filters applying to image levels (Eqs. 2.37–2.38)

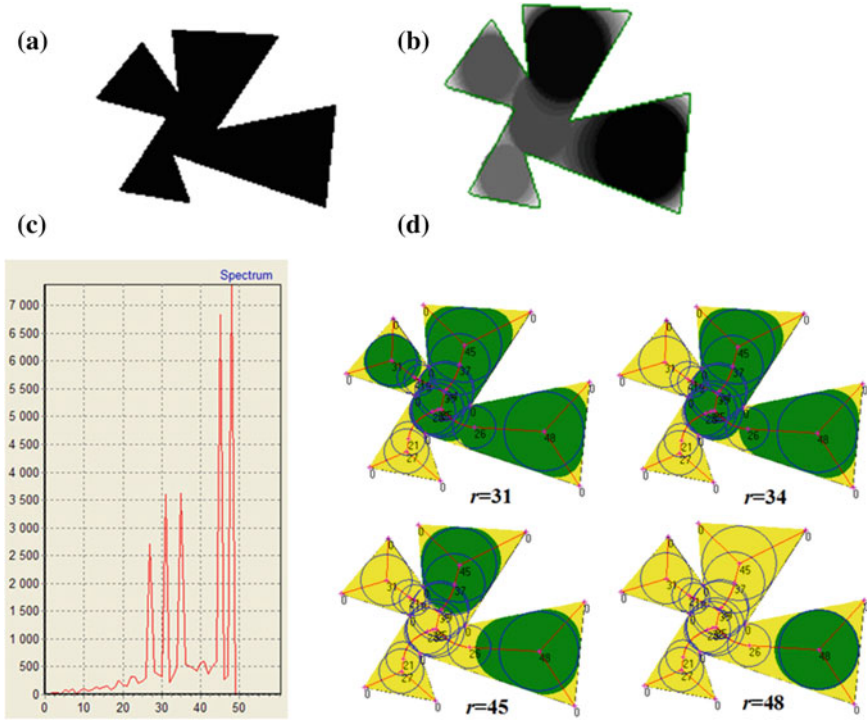


Fig. 2.16 Illustration of DCMPS: **a** the binary image of polygonal figure, **b** the positive part of thickness map, **c** the positive part of DCMPS, **d** the selected parts of figure with minimal width (local thickness) corresponding to essential peaks in a spectrum (results of opening with relevant disk size)

$$f(x, y) \circ b(u, v) = \sum_{l=0, \dots, N} \{f_l(x, y) \circ b(u, v)\} = \max_{l=0, \dots, N} \{l \times f_l(x, y) \circ b(u, v)\} \quad (2.37)$$

$$f(x, y) \bullet b(u, v) = \sum_{l=0, \dots, N} \{f_l(x, y) \bullet b(u, v)\} = \max_{l=0, \dots, N} \{l \times f_l(x, y) \bullet b(u, v)\} \quad (2.38)$$

Therefore, a grayscale spectrum can be calculated as a sum of level spectra by Eqs. 2.39–2.40.

$$PS_f(r, k) = \sum_{l=0, \dots, N-1} PS_{fl}(r, k) \quad (2.39)$$

$$PS_f(-r, k) = \sum_{l=0, \dots, N-1} PS_{fl}(-r, k) \quad (2.40)$$

Thus, the calculation of PS with “flat” disk SE for N -level grayscale image will be N times longer than the computation of the DCMPS for each its binary level image. However, if an approximate spectrum calculation is admissible, the speed of computations can be significantly increased through the use of lower number of binary levels for approximation of the grayscale image. A number n of required approximation levels is determined by a number of significant histogram modes.

Our level selection technique is based on the multimodal generalization of the Otsu bimodal separability criterion. Let us consider the $(n + 1)$ -dimensional vector $\mathbf{t} = (t_0, \dots, t_n)$, where $t_0 = 0$, $t_n = 255$, t_1, \dots, t_{n-1} are free variables corresponding to the thresholds between the histogram modes. If a number of the histogram modes is unknown, then the task of histogram segmentation is, generally speaking, incorrect and requires the regularization [55]. The optimal segmentation corresponds to solution of optimization problem defined by Eq. 2.41, where $\text{DISP}(t_i, t_{i+1})$ is a value of the dispersion of the image histogram fragment on the interval (t_i, t_{i+1}) , α is a regularization parameter.

$$\sum_{i=0, \dots, n} \text{DISP}(t_i, t_{i+1}) + \alpha n \rightarrow \min(n, t_1, \dots, t_{n-1}) \quad (2.41)$$

This problem is solved by the Dynamic Programming (DP) [53]. After that, the approximate morphological spectrum of grayscale image is formed via fast computing and summing of n binary level spectra [53–57]. The negative part of the spectrum (Eq. 2.40) can be calculated using the same algorithm applied to the inverted image (background).

2.5 Morphological Image Analysis (Pyt’ev Morphology)

The basic ideas of Morphological Image Analysis (MIA) are proposed and developed by Pyt’ev since 1960–1970 [58–64]. Further development and generalization of this morphological technique was performed by Pyt’ev, Chulichkov, Kalinin, Loginov, Smolovik, Falomkin, Zhivotnikov, Antonjuk, Zheltov, Vizilter, Rubis, and other researchers of Russian morphological school [65–81].

Let us note that the MIA was proposed approximately at the same time independently and had the proper evolution in parallel way relative to well-known MM proposed by Serra and Matheron [1, 2]. Both terms “morphology” and “morphological analysis” historically belong to both approaches, and they will make some confusion in this chapter. Therefore, for separating MIA from MM, let us refer the MM as the Serra morphology and the MIA as the Pyt’ev morphology (with great respect to all other authors of MM and MIA concepts and results). Unfortunately, basic and some further papers on MIA were published in Russian only, and due to this the Pyt’ev morphology is not so known and popular in the world, but its difference and similarity to the MM are worthy to become a subject of the most fixed consideration.

From practical point of view, the Pyt'ev morphology is basically a technique for invariant and robust image comparison and model-based matching (a template matching in the simplest case). In contrary, the Serra MM is basically a technique for image transforming (a filtering). However, the difference is not only in basic tasks of image analysis. Different classes of objects inspired these morphological approaches in their early days. The Serra morphology was initially developed for binary images of planar figures and then generalized for grayscale and color images. The Pyt'ev morphology was initially developed for comparison of grayscale and color images of 3D scenes. Different target objects produce different concepts of image shape.

From the theoretical point of view, the MIA is another algebraic approach to image shape description and analysis. The Serra morphology is based on non-linear set-theoretic (complete lattice) models. The Pyt'ev morphology is based on vector algebra and functional analysis. Therefore, the monotonous properties (extensive or ant-extensive) of Serra morphological filters (projectors) are not satisfied for Pyt'ev morphological filters (projectors). The Pyt'ev shapes are the rigorous mathematical objects with clear geometrical sense—the hyperplanes in an image space. The Serra shape models have no such interpretation. Due to this, the Pyt'ev morphological correlation coefficient or geometrical correlation coefficients (proposed by Vizilter, Rubis, and Zheltov in the framework of the MIA) have no analogies in the Serra MM. On the other hand, in the Serra MM based on connected filters there are many coincident terms to Pyt'ev notions of shape, shape complexity, and so on. It is important that formally vector algebra and set-theory (Boolean algebra) are the particular cases of the lattice theory. It is important that idempotent operators (projectors) play the central role in both mentioned morphologies. Thus, one can presume some deep unity of these morphological approaches. It was expressed in the formalism of projective morphology in section below.

Now let us start the brief consideration of Pyt'ev morphological ideas. The main purpose of all MIA techniques is the independence of image analysis results on the conditions of image registration. The invariant image properties determine the concept of the image shape. More generally, one can speak about the shape of any data or signal registered by some sensor.

In morphological analysis, it is supposed that any registered signal contains both “important information” about the source signal and the “secondary information” forced by conditions of registration. For example, let us try to explore some 3D scene by means of analysis of its 2D image. An image content depends both on the objects in the scene and the conditions and technique of image acquisition (lighting, weather, season, camera presets, etc.). For the task of 3D scene analysis the information about scene illumination or image acquisition parameters will be “secondary” information. The part of visible information presented in all images of this scene and determined basically by the content of the scene is called a shape of images in this scene. This information should not change, if conditions of scene registration are modified. Therefore, one can speak about the shape of one image, if this image contains the complete “important information” relevant to all images of this fixed scene view.

In order to define the rigorous mathematical notion of image shape, it is required to determine the transformation of the image corresponding to the changes of image acquisition conditions. The invariant of this transformation will be the shape of image. Based on this shape formalization, one can propose the invariant morphological methods for solution of different practical problems of data comparison, matching, recognition, classification, and estimation of sensor parameters for each proper type of signals or data [65, 68, 69].

A model of image shape invariant for transforms is described in Sect. 2.5.1. Scene recognition based on image shape is discussed in Sect. 2.5.2. Section 2.5.3 provides a detection of scene change based on image shape. A scene recognition based on the shape of noisy image is situated in Sect. 2.5.4. A morphological shape matching is given in Sect. 2.5.5.

2.5.1 Image Shape as an Invariant of Image Transforms

Let image f be a function of two variables (x, y) . A domain for definition of this function is called a field of view X , and the value $f(x, y)$ is called the intensity or color of the image at the point $(x, y) \in X$.

For defining the shape of the image, it is need to determine a model of image changing in variations conditions of registration. Let us suppose, for example, that changes in these conditions lead to intensity changes only and are described by Eq. 2.42, where $F(\cdot)$ is the unknown function of pixel-wise intensity transform.

$$g(x, y) = F(f(x, y)) \quad (2.42)$$

Let \mathbf{F} be the class of admissible transformations of the image f , and one can believe that if $F(\cdot) \in \mathbf{F}$, then image $g = F(f)$ will be the other realizable image of this scene corresponding to some certain conditions of registration.

For example, let us suppose that scene objects are the polyhedra with optically homogeneous flat sides. If they are illuminated by the uniform beam of light, then the image of this scene will be the piecewise-constant function in Eq. 2.43.

$$f(x, y) = \sum_{i=1}^N f_i \chi_{F_i}(x, y) \quad (2.43)$$

Here

$$\chi_{F_i}(x, y) = \begin{cases} 1 & \text{if } (x, y) \in A_{F_i} \\ 0 & \text{if } (x, y) \notin A_{F_i} \end{cases}$$

is the indicator function of A_{F_i} , $i = 1, \dots, N$, and the regions A_{F_i} , $i = 1, \dots, N$, with constant intensity form the tessellation of the field of view X :

$$A_{Fi} \cap A_{Fj} = \emptyset, \quad i \neq j, \quad i, j = 1, \dots, N, \quad \bigcup_{i=1}^N A_{Fi} = X.$$

The differences in images of cube captured with different lighting conditions are shown in Fig. 2.17. Figure 2.18 illustrates a mathematical model of cube image and its shape represented as a tessellation of a field of view.

In this case, the class of transforms \mathbf{F} is specified as a class of all (Borel) functions $\{F(\cdot): R_1 \rightarrow R_1\}$. In result of transformation from Eq. 2.42, all sets (regions) of image points with equal intensity on the image f will have the equal intensity on the image g . Therefore, all f image regions of constant intensity (“flat zones” in the Serra MM terms) will preserve their (geometric) shape. However, in some certain special cases, some regions of the field of view X tessellation, which have different intensity on the image f , will merge into one region with constant intensity on the image g . Then the shape of the image g will be simpler than the shape of the image f .

In the described case (polyhedra world with uniform lighting), the invariant of transformations of class \mathbf{F} is a tessellation $\{A_{Fi}\}_{i=1, \dots, N}$ itself. It can be called the shape of the image f . Let us denote the set of all possible images of scene obtained at various registration conditions as follows

$$V_f = \{g = F(f), F \in \mathbf{F}\}.$$

This set can be equivalently considered as a shape of image f .

If V_f is a convex and closed set in the Euclidean space of all images, then there is the one-to-one correspondence between the set V_f and the operator of projection onto this set P_f . This operator can be easily calculated and also called the shape of image f . Obviously, the set of images V_f is invariant with respect to this Pyt’ev morphological projector and defined by Eq. 2.44.

$$P_f: P_f V_f = V_f \quad (2.44)$$

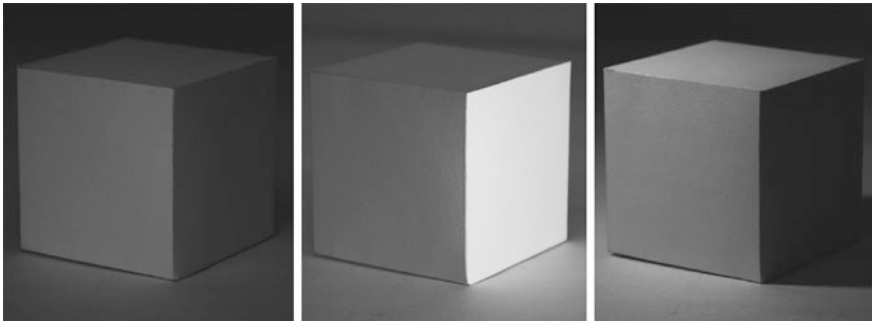


Fig. 2.17 Images of polyhedral world (cube) captured with different lighting conditions

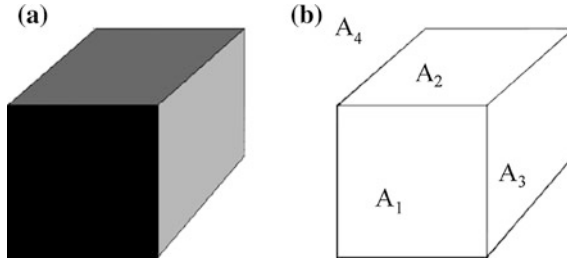


Fig. 2.18 Mathematical model of cube image: **a** a visual model, **b** a shape of cube as a tessellation

Corresponding to Eq. 2.43, an image shape (in this mathematical world) is the linear cover of indicators of regions with equal intensity. From a geometrical point of view, this set of images V_f is a linear subspace (hyperplane) of the Euclidean space of all images. Therefore, a projection of any image g onto the V_f is defined as an orthogonal projection of an image g on this linear subspace.

Constructively, the image projection of g on the set V_f is determined as a solution of the problem of finding best (closest) image in the set V_f to the given image g

$$\|g - P_f g\|^2 = \inf \left\{ \|g - q\|^2 \mid q \in V_f \right\}.$$

For piecewise-constant image f , this problem can be solved in explicit form

$$P_f g = \sum_{i=1}^N \frac{(g, \chi_{F_i})}{\|\chi_{F_i}\|^2} \chi_{F_i}.$$

Let us consider another example. If \mathbf{F} is the class of monotonously increasing functions, than the shape of the image f is a convex cone in Euclidean space of all images. The ordering of values of the intensity of piecewise-constant images is preserved in such monotonous intensity transform model:

$$f(x, y) = \sum_{i=1}^N f_i \chi_{F_i}(x, y), f_1 < f_2 < \dots < f_N \Rightarrow$$

$$F(f) = \sum_{i=1}^N F(f_i) \chi_{F_i}, F(f_1) < F(f_2) < \dots < F(f_N).$$

Local maxima and minima of image intensity are preserved in this shape model. Let us briefly consider some image analysis problems, which can be solved using the Pyt'ev morphology.

2.5.2 Scene Recognition Based on Image Shape

Let image f correspond to scene S registered from some fixed viewpoint by some fixed camera geometry. The inclusion $g \in V_f$ implies that an image g can be an image of the same scene S registered from the same viewpoint with the same camera geometry. The inclusion of $g \in V_f$ is equivalent to the equality $g = P_f g$. This simple condition can be easily and quickly verified.

For any $\varepsilon \geq 0$, the image v is “ ε -similar” to shape of image f , if condition in Eq. 2.45 is executed.

$$\|v - P_f(v)\| \leq \varepsilon \|v\| \quad (2.45)$$

Therefore, the Morphological Correlation Coefficient (MCC) proposed by Pyt'ev has a view of Eq. 2.46.

$$K_m = \frac{\|P_f v\|}{\|v\|} \quad (2.46)$$

The MCC is normalized ($0 \leq K_m \leq 1$) and $K_m = 1$ corresponds to shape equivalence by Eq. 2.47, while $K_m = 0$ corresponds to shape independence by Eq. 2.48, where Πv and Πf are the orthogonal projections of v and f , respectively, onto the set of “flat” images with constant intensity in all points in the field of view X .

$$K_m(v, f) = 1 \Leftrightarrow v \in V_f \Leftrightarrow v = P_f v \quad (2.47)$$

$$\|\Pi v - P_f v\| = 0, \quad \|\Pi f - P_v f\| = 0 \quad (2.48)$$

The coefficient of morphological correlation does not depend on the brightness transform $F(f(x, y))$: $K_m(F(f), f) = 1$. Moreover, if shape of the image v is simpler than shape of the image f , then $K_m(v, f) = 1$.

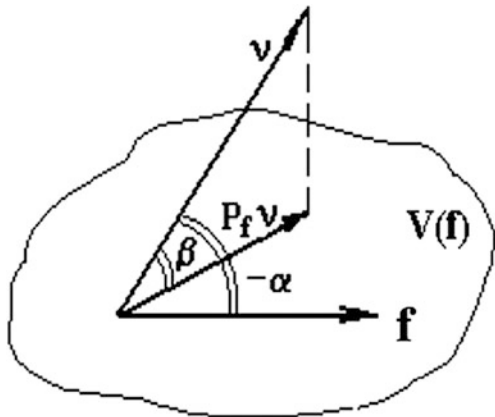
Let us compare this morphological correlation with usual Normalized Correlation (NC) between two images presented in Eq. 2.49.

$$K_u = \frac{(f, v)}{\|f\| \|v\|} \quad (2.49)$$

This NC coefficient is a similarity measure between images taking its values in interval $[-1, 1]$ and invariant relative to class of linear transforms of image intensity: if $v(x, y) = a v(x, y) + b$, then $|K_u(v, f)| = 1$.

A linear transform L is a particular case of arbitrary intensity transform F . Hence, the MCC has greater “invariance power” than the NC: if $K_u = 1$, then $K_m = 1$, but if $K_m = 1$, then K_u should not be equal to 1. Moreover, as it was demonstrated in [74], the MCC is always not less than absolute value of the NC: $K_m \geq |K_u|$. Figure 2.19

Fig. 2.19 Geometrical relation between normalized correlation and morphological correlation, $\alpha = \arccos K_u$, $\beta = \arccos K_m$



illustrates this relation geometrically. The NC is a cosine of angle between v and f in the vector image space. The MCC is a cosine of angle between v and V_f , i.e. between v and $P_f v$. The images are pictured as vectors, and a shape is pictured as a plane (Fig. 2.19). The second angle is always not smaller than the first one, so the MCC is always not less than the NC, and they are equal, if and only if $\|f\|/ \|f\| = P_f v / \|P_f v\|$.

Another difference between the MCC and the NC is that the MCC is not symmetrical relative to v and f : in general case $K_m(v, f) \neq K_m(f, v)$. In particular, if a shape of the image v is simpler than a shape of the image f , then $K_m(v, f) = 1$, but $K_m(f, v) < 1$. The reason of this asymmetry is that the MCC estimates not the similarity between images v and f or between shapes V_v and V_f , but the similarity between image v and shape V_f . So, $\{K_m(v, f) = K_m(v, V_f)\} \neq \{K_m(f, v) = K_m(f, V_v)\}$.

2.5.3 Scene Change Detection Based on Image Shape

Let g and f be the images of the same scene S with some small changes in this scene (some small elements in the scene are added or deleted). If P_f is a projector onto the set of images V_f , then by definition, $P_f g$ is the best approximation of the image g by images from V_f , and hence, $g - P_f g$ is a “morphological difference” of the image g from the shape of image f . This difference is invariant to the conditions of image registration. Thus, the image $g - P_f g$ points to scene changes corresponding to the changes in image g relative to the shape of image f .

The MIA technique is close to the concept of “background normalization” in the MM: the detail extraction uses the difference between initial image and image filtered by morphological filter (projector). Figure 2.20 illustrates this technique for scene change detection in different lighting conditions.

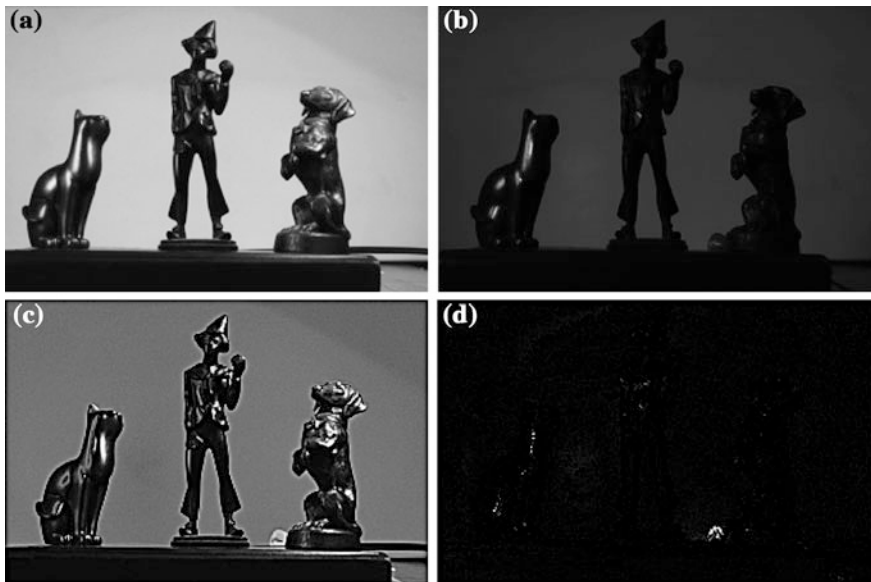


Fig. 2.20 Morphological change detection: **a** the image f determining the shape of scene, **b** the image g with small change in scene content (small bead at the legs of the dog) and strong changes in lighting conditions, **c** a simple difference of f and g (all pixels have changes, so scene changes and intensity changes can not be separated), **d** a morphological difference $g - P_f g$ demonstrates the position of new object (small bead) as an only one bright area

2.5.4 Scene Recognition Based on the Shape of Noisy Image

Let f be the image of scene S_f . Let us consider the registration of corrupted image ζ of some unknown scene: $\zeta = g + v$. Here v is the “noise image”—a model of image corruption by additive noise, and uncorrupted hidden image g is unobservable.

It is required to determine, whether it is possible to consider this image as an image of the scene S_f . For solving this problem in morphological way, let us define the morphological noise-to-signal ratio for image ζ and shape V_f by Eq. 2.50, where $\Pi\zeta$ is the orthogonal projection of ζ onto the set of “flat” images with constant intensity in all points of the field of view X .

$$t(\zeta) = \frac{\|\zeta - P_f \zeta\|^2}{\|\Pi\zeta - P_f \zeta\|^2} \quad (2.50)$$

Consequently, $\Pi\zeta$ is a constant image filled by the average value of intensity of the image ζ . The shorter the distance from ζ to V_f , and more difference of P_f from the constant, the smaller the ratio $t(\zeta)$. The numerator of this ratio contains the squared norm of difference from image ζ to closest image from the set V_f . If $\zeta \notin V_f$, then this difference can be explained only by the presence of noise. The denominator

is the squared norm of the component of image ζ , which is comparable in shape with an image f , and differs from the constant. For decision making about the scene recognition based on images distorted by noise, one needs to specify the threshold value for noise-to-signal ratio.

This brief overview presents the MIA as it was basically proposed. Next paragraphs will be devoted to description of modern generalizations of the MIA, but one needs to note that the MIA approach itself is still under development and able to generate some essentially new ideas. For example, in [82] the new MIA concepts of morphological oblique projectors and relative shapes are proposed by Pyt'ev for the morphological analysis of classes of images and for comparative analysis of their shapes as invariants (under image acquisition conditions). These concepts are used to characterize morphological dependences. More specifically, the relative shapes are characterized by the morphological independence index, and the absolute shapes, by the morphological connection index. New methods based on the constructs of relative shapes of image classes and on the oblique projection technique are described in [82] applying to the comparative analysis of absolute and relative shapes of image classes, the morphological filtration of images, the identification of images, the determination of unknown objects in scene images, and other problems.

2.5.5 Morphological Shape Matching

This subsection addresses the problem of image matching “just by shape” with no dependence on the concrete pixel values. For example, one can compare images of one scene captured at different seasons, time of day, weather and lighting conditions, spectral ranges, etc.

The most popular technique for such image shape comparison utilizes the Mutual Information (MI) measure based on probabilistic reasoning and information theory [83]. A mutual information $I(A, B)$ estimates the dependence of two random variables A and B by measuring the distance between the joint distribution $p_{AB}(a, b)$ and the distribution of complete independence $p_A(a)p_B(b)$ provided by Eqs. 2.51–2.53, where $H(A)$ is an entropy of A , $H(B)$ is an entropy of B , $H(A, B)$ is their joint entropy.

$$I(A, B) = H(A) + H(B) - H(A, B) \quad (2.51)$$

$$H(A) = - \sum_a p_A(a) \log p_A(a) \quad H(B) = - \sum_b p_B(b) \log p_B(b) \quad (2.52)$$

$$H(A, B) = - \sum_a \sum_b p_{AB}(a, b) \log p_{AB}(a, b) \quad (2.53)$$

For two image intensity values a and b of a pair of corresponding pixels in two images, required empirical estimations for the joint and marginal distributions can

be obtained by normalization of the joint (2D) and marginal (1D) histograms of compared image fragments. Maximal $I(A, B)$ value corresponds to the best geometrical matching of image fragments.

Such MI approach provides the robust tool for matching of images with different intensities based on their joint 2D histograms. But these histograms cannot explain the geometrical idea of image “shape” in some evident form. Such mathematical “shape” formalism is given in evident form in the morphological approach to image comparison proposed by Pyt’ev [62].

The Pyt’ev morphological comparison of images $f(x, y)$ and $g(x, y)$ is performed using the MCC $K_M(g, V_f)$ and $K_M(f, V_g)$. This comparison is invariant relative to intensity transforms. However, the Pyt’ev MCC estimates the closeness of image to the shape of other image, but not the similarity of two shapes. Morphological tools for shape matching were proposed by Vizilter, Rubis, and Zheltov [84, 85]. The original Pyt’ev morphological approach was generalized for obtaining the pure “geometry-to-geometry” shape matching technique. In [85], the transform distance for geometrical difference evaluation of shapes named Geometrical Difference Index (GDI) was proposed and normalized similarity measure of image shapes based on GDI was defined. These new morphological tools were experimentally compared with the Pyt’ev MCC and the MI applying to multispectral image matching problem.

In [81], the geometrical shape comparison approach was developed based on Pyt’ev’s morphological image analysis. Let $f(x, y)$ from V_f is a piecewise-constant 2D function described above. Image $g(x, y)$ from V_g is an analogous 2D function with m as a number of tessellation regions $\{A_{G1}, \dots, A_{Gm}\}$, $\mathbf{g} = (g_1, \dots, g_m)$ is a vector of intensity values, $\chi_{Gj}(x, y) \in \{0, 1\}$ is a support function of j th region.

For brevity in this subsection, let us use the following notation: $F = V_f$ and $G = V_g$ for shapes, $F_i = A_{Fi}$ and $G_j = A_{Gj}$ for tessellation regions, $f_G = P_g f$ and $g_F = P_f g$ for projections. Let us also introduce following additional set of “S-variables”: S is an area of the whole frame Ω , $S_i = \|\chi_{Fi}(x, y)\|^2$ is an area of tessellation region F_i , $S_j = \|\chi_{Gj}(x, y)\|^2$ is an area of tessellation region G_j , $S_{ij} = (\chi_{Fi}(x, y), \chi_{Gj}(x, y))$ is an area of intersection $F_i \cap G_j$. With account of these S-variables, one can receive the equations mentioned below.

$$\begin{aligned} \|f\|^2 &= \sum_{i=1, \dots, n} f_i^2 S_i & \|f_G\|^2 &= \sum_{j=1, \dots, m} f_{Gj}^2 S_j \\ f_{Gj} &= \left(\sum_{i=1, \dots, n} f_i S_{ij} \right) / S_j & j &= 1, \dots, m \end{aligned}$$

Let us add the following assumptions about the distributions of probability densities for intensity values f_1, \dots, f_n :

1. If $p(f_1, \dots, f_n) = p(f_1) \dots p(f_n)$, then values f_1, \dots, f_n are independent in general.
2. If $p(f_1) = \dots = p(f_n)$, then values f_1, \dots, f_n are equally distributed.

3. If $\forall i = 1, \dots, n: p(f_i) = p(-f_i)$, then values f_1, \dots, f_n are distributed symmetrically to 0.

Then the expectation $\langle f_i \rangle = 0, i = 1, \dots, n$ and the covariance has the form of Eq. 2.54, where σ is a dispersion of probability distribution $p(f_i)$.

$$\langle f_i f_k \rangle = \begin{cases} \sigma^2 & \text{if } i = k \\ 0 & \text{otherwise} \end{cases} \quad (2.54)$$

Thus, the mean square of norm for image f of shape F has a form of Eq. 2.55.

$$\langle \|f\|^2 \rangle = \sum_{i=1}^n \langle f_i^2 \rangle S_i = \sum_{i=1}^n \sigma^2 S_i = \sigma^2 \sum_{i=1}^n S_i = \sigma^2 S \quad (2.55)$$

The mean square of projection norm for image $f \in F$ and fixed shape G has a form of Eq. 2.56.

$$\begin{aligned} \langle \|f_G\|^2 \rangle &= \sum_{j=1}^m \langle f_{Gj}^2 \rangle S_j = \sum_{j=1}^m \left\langle \left(\sum_{i=1}^n f_i S_{ij} \right)^2 / S_j^2 \right\rangle \\ S_j &= \sum_{j=1}^m \left(\sum_{i=1}^n \sigma^2 S_{ij}^2 \right) / S_j = \sigma^2 \sum_{j=1}^m \sum_{i=1}^n S_{ij}^2 / S_j \end{aligned} \quad (2.56)$$

Let us define the Mean Square Effective Morphological Correlation Coefficient (MSEMCC) for shapes $F = V_f$ and $G = V_g$ provided by Eq. 2.57.

$$K_M^2(F, G) = \frac{\langle \|f_G\|^2 \rangle}{\langle \|f\|^2 \rangle} \quad (2.57)$$

After evident substitutions, the MSEMCC takes the compact form by Eq. 2.58, where $K_\Omega(F_i, G_j) = S_{ij}/S$ is a normalized influence coefficient for pair of regions F_i and G_j , $K_M^2(G_j, F_i) = S_{ij}/S_j$ is a square of normalized morphological correlation for this pair of regions.

$$K_M^2(F, G) = \sum_{j=1}^m \sum_{i=1}^n \frac{S_{ij}}{S} \frac{S_{ij}}{S_j} = \sum_{j=1}^m \sum_{i=1}^n K_\Omega(F_i, G_j) K_M^2(G_j, F_i) \quad (2.58)$$

In [85], the special transform distance for geometrical difference evaluation of shapes named GDI was proposed and some normalized similarity measures of image shapes based on the GDI were presented. The GDI metrics for two image shapes F and G are defined by Eqs. 2.59–2.61.

$$d_H(F, G) = \sum_{j=1}^m \sum_{i=1}^n p_{ij} d_H(G_j, F_i) \quad (2.59)$$

$$d_H(G_j, F_i) = p_i + p_j - 2p_{ij} \quad (2.60)$$

$$p_{ij} = S_{ij}/S, p_i = S_i/S, p_j = S_j/S \quad (2.61)$$

Most useful the GDI-based similarity measure proposed in [85] is a Centered Metrical Similarity Coefficient (CMSC), which is based on comparison with assumption about F and G shapes independence. In this case $d_{HInd}(\cdot)$ has a view below.

$$d_{HInd}(F, G) = \sum_{j=1}^m \sum_{i=1}^n p_i p_j (p_i + p_j - 2p_{ij})$$

Therefore, the CMSC is defined by Eq. 2.62.

$$K_{CHS}(F, G) = \frac{|d_{HInd}(F, G) - d_H(F, G)|}{d_{HInd}(F, G)} \quad (2.62)$$

The CMSC has the following properties:

1. $K_{CHS}(F, G) \in [0, 1]$.
2. $K_{CHS}(F, G) = 1 \Leftrightarrow F = G$.
3. $K_{CHS}(F, G) = K_{CHS}(G, F)$.
4. $\forall i, j: p_{ij} = p_i p_j \Rightarrow K_{CHS}(F, G) = 0$.

For comparison of geometrical correlation techniques and corresponding similarity measures, the MI criterion and the Pyt'ev's MCC were calculated over a set of real images including remote sensing and multispectral images [TeleVision (TV) and InfraRed (IR)] [86]. In all experiments, both the Pyt'ev MCC and geometrical correlation measures (Eqs. 2.58, 2.62) provide matching characteristics (signal-to-noise ratio and elevation of main peak in a correlation field) close to mutual information characteristics (a little bit worse or better). In the case of small TV fragments and noisy IR images, the characteristics of the CMSC (Eq. 2.62) were better than Pyt'ev's morphological coefficient and mutual information characteristics. Figures 2.21 and 2.22 demonstrate the example of such TV-IR matching test and corresponding correlation fields. From the computational viewpoint, the geometrical correlation outperforms the mutual information in calculation speed about 20 %.

Thus, the morphological techniques for change detection and scene recognition are invariant relative to conditions of image registration.

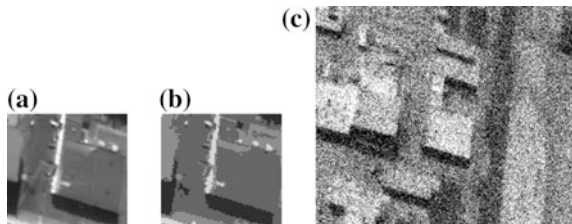


Fig. 2.21 Example of TV-IR matching: **a** a TV etalon, **b** a segmented TV fragment, **c** test IR

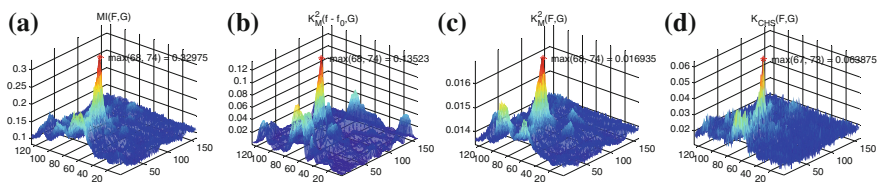


Fig. 2.22 Correlation fields for TV-IR matching: **a** the mutual information $MI(F, G)$, **b** the square of centered Pyt'ev MCC $K_M^2(f - f_0, G)$, **c** the square of MSEMCC $K_M^2(F, G)$, **d** the square of CMSC $K_{CHS}^2(F, G)$

2.6 Projective Morphologies, Morphological Segmentation and Complexity Analysis

The projective morphology approach was developed based on the Serra MM [1], the Pavel shape theory [87], and the Pyt'ev MIA [62]. It presumes structural image modeling with regularization constrains. This section describes the image segmentation problem from the morphological point of view and introduces the criterion-based morphological filters (projectors) and morphological spectra based on regularization and analysis of shape complexity [79, 80, 84, 88]. The corresponding morphological tools have been successfully applied for different practical computer vision tasks [89–95].

Section 2.6.1 provides the projective morphologies based on morphological decompositions. The image segmentation in the framework of projective morphology is represented in Sect. 2.6.2. The shape regularization and morphological filters are discussed in Sect. 2.6.3. The morphological complexity and filters and spectra by complexity are introduced in Sect. 2.6.4.

2.6.1 Projective Morphologies Based on Morphological Decompositions

The projective space of patterns (images) is as an algebraic system $\langle \Psi, \Omega, \cdot, \vee, \mu, Pr, E \rangle$, where Ψ is a set of scalars including 0 and 1, Ω is the set of patterns with

“zero pattern” \emptyset , ‘ \cdot ’ is the multiplicative group operation of multiplication of scalars $\Psi \times \Psi \rightarrow \Psi$ and a scalar by pattern multiplication $\Psi \times \Omega \rightarrow \Omega$, ‘ \vee ’ \in {‘ $+$ ’, ‘ \times ’, ‘ \cup ’, ‘ \cap ’, ‘ \vee ’, ‘ \wedge ’, ‘ \min ’, ‘ \max ’, ...} is the additive Abel semi-group of scalars fusion $\Psi \times \Psi \rightarrow \Psi$ and patterns fusion $\Omega \times \Omega \rightarrow \Omega$, μ is the norm of the pattern $\Omega \rightarrow \mathbb{R}$ ($\mu(A) = \|A\|$, $\|\emptyset\| = 0$), set of basic patterns (primitives) $\mathbf{E} = \{E_1, \dots, E_n\}$ is the basis of the morphological pattern decomposition. Let \mathbf{E} denote the corresponding morphological subspace $\mathbf{E} \subseteq \Omega$ generated by the algebraic closure of basis \mathbf{E} relative to ‘ \cdot ’, ‘ \vee ’-combination.

The operator of linear projection of pattern onto the pattern has a form of Eq. 2.63, where $r(A, B) \in \Psi$ is the coefficient of linear dependence of pattern A relative to pattern B .

$$Pr(A, B) = r(A, B) \cdot B: \Omega \rightarrow \mathbf{B} \subseteq \Omega \quad (2.63)$$

The projection of pattern onto subspace

$$Pr(A, \mathbf{E}): \Omega \rightarrow \mathbf{E} \subseteq \Omega, Pr(A, \mathbf{E}) = Pr(Pr(A, \mathbf{E}), \mathbf{E})$$

is the idempotent operator satisfying the decomposition condition Eq. 2.64, where $\mathbf{a}(A, \mathbf{E}) = \langle r(A, E_k) \rangle_{k=1, \dots, n}$ is the vector of morphological decomposition of pattern A in basis \mathbf{E} .

$$Pr(A, \mathbf{E}) = \bigvee_{k=1, \dots, n} Pr(A, E_k) = \bigvee_{k=1, \dots, n} r(A, E_k) \cdot E_k \quad (2.64)$$

The morphological decomposition is a mapping defined by Eq. 2.65.

$$\mathbf{dec}_{\mathbf{E}}(A) = \langle r(A, E_1), \dots, r(A, E_n) \rangle: \Omega \rightarrow \Psi^n \quad (2.65)$$

2.6.2 Image Segmentation in the Framework of Projective Morphology

Let the morphological descriptor of pattern $A \in \Omega$ be a data structure of the form of Eq. 2.66, where $\mathbf{E} = \langle E_1, \dots, E_n \rangle \in \Omega^n$ is a basis of decomposition, $n = \dim(\mathbf{E})$ is the dimension of \mathbf{E} , $d(A, E_i)$ is the descriptor of decomposition element.

$$\mathbf{d}(A, \mathbf{E}) = \langle n, d(A, E_1), \dots, d(A, E_n) \rangle \quad (2.66)$$

The descriptor size $v(\mathbf{d})$ is a memory size required for storing of descriptor \mathbf{d} (Eq. 2.66). The basis \mathbf{X} of decomposition is complete on Ω if $\forall A \in \Omega: Pr(A, \mathbf{X}) = A$. Then for any $A \in \Omega$ its descriptor $\mathbf{d}(A, \mathbf{X})$ is a complete descriptor. Any subbasis $\mathbf{Y} = \langle Y_1, \dots, Y_m \rangle: \mathbf{Y} \subseteq \mathbf{X}$, $\dim(\mathbf{Y}) \leq \dim(\mathbf{X})$ determines a subdescriptor $\mathbf{d}(A, \mathbf{Y})$. The set $\Theta(\mathbf{X}) = \{\mathbf{d}(A, \mathbf{Y}): A \in \Omega, \mathbf{Y} \subseteq \mathbf{X}\}$ is a set of all subdescriptors based on \mathbf{X} .

In the framework of shape theory [87], the morphological segmentation operator can be stated as a mapping of pattern from Ω to subdescriptor from $\Theta(\mathbf{X})$ provided by Eq. 2.67.

$$\varepsilon_s: \Omega \rightarrow \Theta(\mathbf{X}) \quad (2.67)$$

The operator of morphological reconstruction is defined in a following view

$$\delta_s: \Theta(\mathbf{X}) \rightarrow \Omega.$$

Therefore, their combinations will be the morphological filter, and algebraic projector is computed by Eq. 2.68.

$$Pr(A, \Theta(\mathbf{X})) = \psi_s \quad A = \delta_s \varepsilon_s A \quad \psi_s: \Omega \rightarrow \Omega \quad \psi_s^2 = \psi_s \quad (2.68)$$

Let us define a segmentation criterion or shape cost function with regularization parameter α in the form of Eq. 2.69, containing a penalty both for the descriptor size v (complexity criterion) and for deviation of projected pattern from the initial pattern J (reconstruction criterion).

$$\Phi(A, \mathbf{Y}) = J(A, Pr(A, \mathbf{Y})) + \alpha \times v(\mathbf{d}(A, \mathbf{Y})) \rightarrow \min(\{Y: Y \subseteq X\}) \quad (2.69)$$

The optimal morphological segmentation finds an optimal subbasis \mathbf{Y} (Eq. 2.70).

$$\varepsilon_\Phi(A, \mathbf{X}) = \operatorname{argmin}_{\mathbf{Y}} \Phi(A, \mathbf{Y}) \quad (2.70)$$

Then the pattern A as its projection on this subbasis is reconstructed by Eq. 2.71.

$$\psi_\Phi(A, \mathbf{X}) = Pr(A, \varepsilon_\Phi(A, \mathbf{X})) \quad (2.71)$$

In particular, the segmentation without losses provides the exact reconstruction by Eq. 2.72.

$$\varepsilon_v(A, \mathbf{X}) = \operatorname{argmin}_{\mathbf{Y}} \{v(\mathbf{d}(A, \mathbf{Y})): Y \subseteq X \quad Pr(A, \mathbf{Y}) = A\} \quad \psi_v(A, \mathbf{X}) = A \quad (2.72)$$

The segmentation without losses presumes the construction of optimal basis via elimination of zero-coefficient primitives and grouping of equal-coefficient primitives. Each morphological system has the special constraints on grouping.

Example 1 Let initial complete decomposition \mathbf{X} be a pixel tessellation (Eq. 2.73), where $\varphi(i, j, x, y)$ is an indicator function of pixel (x, y) , $a_{ij} = f(i, j)$.

$$f(x, y) = \sum_{ij} a_{ij} \varphi(i, j, x, y) \quad (2.73)$$

The segmentation scheme without losses is based on grouping of neighbor pixels with equal values. This scheme automatically generates the Pyt'ev morphological

shape [62] as an orthogonal projective decomposition of the form of Eq. 2.74, where $\chi_i \in \{0, 1\}$ is an indicator function of i th connected region with intensity a_i .

$$f(x, y) = \sum_{i=1, \dots, n} a_i \cdot \chi_i(x, y) \quad (2.74)$$

Example 2 A granulometry based on the binary Serra MM with disk SE provides a monotonous projective decomposition with operation ‘V’ = ‘U’ and complete basis of binary structuring elements $D(x, y, R)$. In this case, the segmentation scheme without losses is based on following rule for grouping of structuring elements: the greater disks absorb the smaller ones that completely belong to them. Thus, the segmentation provides a minimal set of inscribed disks recovering the pattern A . In other words, this segmentation scheme automatically generates a morphological shape descriptor based on a skelitonization technique.

2.6.3 Shape Regularization and Morphological Filters by Regularization

If optimal segmentation $\varepsilon_{\Phi}(A, \mathbf{X})$ may return the subbasis \mathbf{Y} such that $Pr(A, \mathbf{Y}) \neq A$, then such scheme is called the segmentation with losses or shape regularization. If the operator of shape regularization $\psi_{\Phi}(A, \mathbf{X})$ is idempotent (projector), then it is a morphological filter by regularization. For some certain forms of regularization criterion the projectivity of segmentation operator can be proved. The first type of projective segmentation is a minimal distance regularization provided by Eq. 2.75, where a distance $\rho(A, B) = \|A - B\|$ satisfies the metrics properties by Eq. 2.76.

$$\Phi(A, \mathbf{Y}) = \|A - Pr(A, \mathbf{Y})\| + \alpha \times v(\mathbf{d}(A, \mathbf{Y})) \rightarrow \min(\mathbf{Y}: \mathbf{Y} \subseteq \mathbf{X}) \quad (2.75)$$

$$\forall A, B, C \in \Omega: \rho(A, B) \geq 0, \rho(A, A) = 0, \quad \rho(A, B) + \rho(B, C) \leq \rho(A, C) \quad (2.76)$$

Additionally assume that for any basis \mathbf{E} Eq. 2.77 is executed.

$$\forall A \in \Omega: B = Pr(A, \mathbf{E}) \Leftrightarrow B \in \mathbf{E} \quad \forall C \in E: \|A - B\| \leq \|A - C\| \quad (2.77)$$

As it was proved in [96], the operators $\psi_{\Phi}(A, \mathbf{X})$ satisfying Eqs. 2.75 and 2.77 are idempotent and called the minimal distance projectors (in particular, the Pyt'ev projector from Example 1). Thus, one can speak about a class of morphological systems $\langle \mathbf{X}, \alpha, v, \rho \rangle$ based on a distance ρ , a basis \mathbf{X} , a weight parameter α , and a descriptor size $v(\mathbf{d}(\mathbf{Y}))$.

Example 3 The minimal L1-distance segmentation of 2D functions using Dynamic Programming technique (DP-segmentation) requires the description of 2D image structure by some non-circular graph (tree). Such projective segmentation scheme based on level set trees is described in [97] (see Fig. 2.23).

The second type of projective segmentation is a monotonous regularization provided by Eq. 2.78 or Eq. 2.79, where $A \leq B \Leftrightarrow \forall x, y: A(x, y) \leq B(x, y)$.

$$\forall A, \mathbf{X}: \psi_{\Phi}(A, \mathbf{X}) = Pr(A, \varepsilon_{\Phi}(A, \mathbf{X})) \leq A \quad (2.78)$$

$$\forall A, \mathbf{X}: \psi_{\Phi}(A, \mathbf{X}) = Pr(A, \varepsilon_{\Phi}(A, \mathbf{X})) \geq A \quad (2.79)$$

As it was proved in [96], for any convex criterion J operators $\psi_{\Phi}(A, \mathbf{X})$ satisfying Eqs. 2.78–2.79 are idempotent and called the regularization opening and the regularization closing, respectively. Therefore, one can speak about morphological systems $\langle \mathbf{X}, \alpha, v, J \rangle$ based on an initial basis \mathbf{X} , a weight parameter α , a descriptor size $v(\mathbf{d}(\mathbf{Y}))$, and a reconstruction cost $J(Pr(A, \mathbf{Y}))$.

Example 4 The monotonous segmentation of 1D и 2D functions using the DP technique is similar to one in Example 3 with account of Eq. 2.78 for DP-opening and Eq. 2.79 for DP-closing. Note, that filters in Examples 3 and 4 are the connected filters of the Serra MM.

The DP is not the only effective programming techniques for solution of morphological segmentation tasks. Very efficient solutions can be obtained using the linear programming, the graph cut technique [98–103] and the Hough-like transforms (see Example 5) (Fig. 2.24)

Example 5 A morphological segmentation based on the Hough transform [88] is proposed in [104]. It includes the following steps:

- Step 1: The application of the Hough Transform (HT).
- Step 2: The binarization of the Hough accumulator with fixed threshold value t .
- Step 3: The deletion all dots of source dot pattern, which are not on detected as straight lines.

Such procedure defines the Hough-projector (the Hough-opening MM filter). The optimal segmentation problem is reduced to search of optimal segmentation parameter $t_{\text{opt}} = t(\alpha)$. This approach can be easily expanded to any generalization or modification of the HT. For example, the Recurrent Hough Transform (RHT) in a



Fig. 2.23 The projective DP-segmentation of grayscale image by level set tree with L1-distance criterion and regularization parameter α producing different number of support regions n : **a** $\alpha = 0$, $n = 1,395$, **b** $\alpha = 1,000$, $n = 102$, **c** $\alpha = 10,000$, $n = 23$, **d** $\alpha = 1,000,000$, $n = 2$



Fig. 2.24 Projective monotonous DP-opening of grayscale image by level set tree with regularization parameter α producing different number of support regions n : **a** $\alpha = 0$, $n = 1,584$, **b** $\alpha = 1,000$, $n = 120$, **c** $\alpha = 10,000$, $n = 24$, **d** $\alpha = 100,000$, $n = 8$

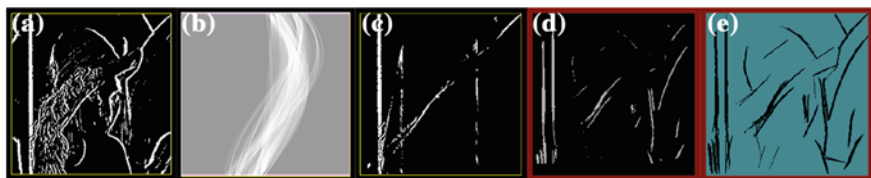


Fig. 2.25 Examples of Hough and RHT-opening: **a** the initial binary image, **b** the Hough accumulator, **c** the Hough-opening (global linear structures are detected), **d** the RHT accumulator, **e** the RHT-opening (local linear structures are extracted)

sliding window produces the morphological RHT-opening [104]. The examples of the Hough-opening and the RHT-opening are shown in Fig. 2.25.

2.6.4 Morphological Complexity, Filters, and Spectra by Complexity

The morphological regularization can be generalized in terms of the morphological complexity proposed by Pyt'ev. Let us consider two projectors φ_1 and φ_2 and corresponding to Pyt'ev shapes (sets of stable elements of projectors). If a shape M_1 contains shape M_2 (i.e. filter φ_1 preserves all patterns filtered by φ_2), then the shape M_1 has less (not greater) morphological complexity than shape M_2

$$M_1 = \{\varphi_1 A : A \in \Omega\}, \quad M_2 = \{\varphi_2 A : A \in \Omega\}: M_2 \subseteq M_1 \Rightarrow \varphi_1 \varphi_2 = \varphi_2.$$

Usually one can speak and think about the structural complexity of patterns: the greater numbers of elements is used in a model of shape, the more complex model is formed. But such complexity definition requires some structural description (for example, in terms of morphological decompositions). In contrast, morphological complexity definition does not require any structural description. It operates just

with projectors and corresponding stable sets but can be easily interpreted in any certain morphological system. For example, if one frame tessellation is a partition of other frame tessellation, it will be relatively more complex both in structural (a number of elements corresponds to a region) and in morphological sense (based on comparison of Pyt'ev projectors). In the case of the Serra MM with disk SE opening, the smaller size of disk corresponds to more complex shape than opening with greater size of disk in both senses: larger number of small disks required for reconstruction and opening with smaller disk preserves results of opening with greater disk.

Thus, one can define the morphological complexity regularization criterion in the most general form (free of structural morphological decomposition terms) provided by Eq. 2.80, where $A, L \subseteq \Omega$ are original and reconstructed patterns correspondingly, $J(A, L)$ is a precision of reconstruction, $Q(L)$ is a complexity of reconstruction, $\alpha \geq 0$ is a parameter of morphological complexity of the operator ψ_α , regulating a compromise between J and Q .

$$F_\alpha(A, L) = J(A, L) + \alpha Q(L) \quad (2.80)$$

The corresponding morphological filter by complexity is defined by Eq. 2.81.

$$\psi_\alpha A = \operatorname{argmin}_{L \in \Omega} F_\alpha(A, L) \quad (2.81)$$

In general, $J(A, L)$ can be any function of L that is monotonously growing with complexity $Q(L)$. The corresponding morphological spectrum by complexity is defined as a derivative of J by complexity parameter α in Eq. 2.82.

$$PS(A, \alpha) = \partial J(A, \psi_\alpha A) / \partial \alpha \quad (2.82)$$

Such definitions are more general than definitions of morphological filters and spectra based on granulometry sieving or any other structural models considered in the MM. Thus, the notions of morphological filters by complexity and morphological spectra by complexity proposed in [105] provide the most general morphological tool for shape analysis based on shape complexity.

2.7 Conclusion

Some original and modern morphological concepts and tools were presented in this chapter as well as required amount of morphological basics. The morphological techniques, which are applicable for real-time technical vision systems, were selected and presented. The continuous skeleton is described by the strict mathematical model. A computation time of continuous skeletonization algorithm outperforms the best samples of discrete skeletonization algorithms by a factor of ten or even hundred. If a figure is polygonal, then continuous skeletonization represents

it as a union of finite number of ANalytical struCTure ELements (anxels). Such anxel representation allows to define different continuous binary morphologies based on selection and/or transformation of figure or background anxels. The effective approach to the calculation of morphological pattern spectra of binary and grayscale images with the disk structuring elements is described. It is based on the continuous skeletal representation, the thickness map concept and the level decomposition of morphological spectra.

Morphological image analysis (Pyt'ev morphology) is described. The Pyt'ev morphology is developed for matching and comparison of grayscale and color images of 3D scenes. It is based on vector algebra and functional analysis. The Pyt'ev shapes are the hyperplanes in an image space. Morphological techniques for change detection and scene recognition based on image-to-shape and shape-to-shape similarity estimation are described. These techniques are invariant relative to conditions of image registration.

The projective morphology is described as a generalized framework based on the Serra morphology, the Pavel shape theory, and the Pyt'ev morphological analysis. The projective morphology combines ideas of these morphological approaches and allows to construct some new morphological systems and operators based on different image decompositions, transforms, and criterions (energy functions). The morphological shape complexity as a criterion for shape regularization is the basis of tools for shape complexity analysis.

Acknowledgments Authors thank all colleagues from Moscow Morphological Workshop in the Lomonosov Moscow state university (supervised by Prof. Y. Pyt'ev) for many-years fruitful and kind discussions. Special thanks are to Russian Fund of Basic Researches supported the morphological researches by a series of grants.

References

1. Serra J (1982) Image analysis and mathematical morphology. Academic Press, London
2. Matheron G (1975) Random sets and integral geometry. Wiley, New York
3. Serra J (1988) Image analysis and mathematical morphology. Theoretical advances. Academic Press, London
4. Dougherty ER (1992) An introduction to morphological image processing. SPIE Optical Engineering Press, Bellingham, Washington, USA
5. Najman L, Talbot H (2010) Mathematical morphology: from theory to applications. Wiley, Hoboken, NJ
6. Serra J, Soille P (1994) Mathematical morphology and its applications to image processing. Kluwer Academic Publishers, Dordrecht
7. Shih FY, Mitchell OR (1989) Threshold decomposition of gray scale morphology into binary morphology. IEEE Trans Pattern Anal Mach Intell 11(1):31–42
8. Grätzer G (2011) Lattice theory: foundation Springer Basel
9. Nachtgaelel M, Sussner P, Mélangé T, Kerre E (2011) On the role of complete lattices in mathematical morphology: from tool to uncertainty model. Inf Sci 181(10):1971–1988
10. Ronse C, Najman L, Decencière E (eds) (2005) Mathematical morphology: 40 years on 7th international symposium on mathematical morphology, vol 30

11. Salembier P, Wilkinson MHF (2009) Connected operators: a review of region-based morphological image processing techniques. *IEEE Signal Process Mag* 26(6):136–157
12. Vizilter YV (2002) Design of morphological operators based on selective morphology. In: Dougherty ER, Astola JT, Egiazarian KO (eds) *Proceedings of SPIE—the international society for optical engineering image processing: algorithms and systems*, pp 215–226
13. Lantuéjoul Ch (1977) Sur le modèle de Johnson-Mehl generalize. Internal report of the Centre de Morph. Math., Fontainebleau, France
14. Aichholzer O, Aurenhammer F (1996) Straight skeletons for general polygonal figures in the plane. In: Cai JY, Wong CK (eds) *Computing and combinatorics*, vol 1090. LNCS Springer, pp 117–126
15. Blum H (1967) A transformation for extracting new descriptors of shape. In: Wathen-Dunn W (ed) *Models for the perception of speech and visual form*, pp 362–380
16. Costa L, Cesar R (2001) *Shape analysis and classification*. CRC Press, USA
17. Siddiqi K, Pizer SM (2008) *Medial representations: mathematics, algorithms and applications*. Springer, Berlin
18. Mestetskiy L (2006) Skeletonization of a multiply connected polygonal domain based on its boundary adjacent tree. *Siberian J Numer Math* 9(3):299–314 (in Russian)
19. Mestetskiy L (2007) Shape comparison of flexible objects—similarity of palm silhouettes. In: 2nd international conference on computer vision theory and applications VISAPP'2007, pp 390–393
20. Mestetskiy L (2009) Continuous morphology of binary images: figures, skeletons and circulars. *Fizmatlit, Moscow* (in Russian)
21. Mestetskiy L (2010) Skeleton representation based on compound Bezier curves. In: 5th International conference on computer vision theory and applications VISAPP'2010, vol 1. INSTICC Press, pp 44–51
22. Mestetskiy L, Semenov A (2008) Binary image skeleton—continuous approach. In: 3rd international conference on computer vision theory and applications VISAPP'2008, vol 1. INSTICC Press, pp 251–258
23. Deng W, Iyengar S, Brener N (2000) A fast parallel thinning algorithm for the binary image skeletonization. *Int J High Perform Comput Appl* 14(1):65–81
24. Drysdale R, Lee D (1978) Generalized Voronoi diagrams in the plane. In: 16th Ann Allerton conference on communications, control and computing, pp 833–842
25. Kirkpatrick D (1979) Efficient computation of continuous skeletons. In: 20th Ann IEEE symposium foundations of computer science, pp 18–27
26. Fortune S (1987) A sweepline algorithm for Voronoi diagrams. *Algorithmica* 2:153–174
27. Yap C (1987) An $O(n \log n)$ algorithm for the Voronoi diagram of the set of simple curve segments. *Discrete Comput Geom* 2:365–393
28. Lee D (1982) Medial axis transformation of a planar shape. *IEEE Trans Pattern Anal Mach Intell PAMI-4* 4:363–369
29. Lee DT, Schachter BJ (1980) Two algorithms for constructing a Delaunay triangulation. *Int J Comput Inf Sci* 9(3):219–242
30. Manzanera A, Bernard T, Preteux F, Longuet B (1999) Ultra-fast skeleton based on an isotropic fully parallel algorithm. In: Bertrand G, Couprie M, Perrotin L (eds) *Discrete geometry for computer imagery*, vol 1568. LNCS Springer, Berlin, pp 313–324
31. Karavelas MI (2006) Voronoi diagrams in CGAL. In: 22nd European workshop on computational geometry, pp 229–232
32. Srinivasan V, Nackman L, Tang J, Meshkat S (1992) Automatic mesh generation using the symmetric axis transform of polygonal domains. *Proc IEEE* 80(9):1485–1501
33. Ogniewicz R, Kubler O (1995) Hierarchic Voronoi skeletons. *Pattern Recogn* 28(3):343–359
34. Strzodka R, Telea A (2004) Generalized distance transforms and skeletons in graphics hardware. *Joint eurographics—IEEE TCVG symposium on visualization*
35. Maragos P (1989) Pattern spectrum and multiscale shape representation. *IEEE Trans Pattern Anal Mach Intell* 11:701–715

36. Suruliandi A, Ramar K (2008) Local texture patterns—a univariate texture model for classification of images. In: 16th IEEE International conference on advanced computing and communications, ADCOM 2008, pp 32–39
37. Asano A (1999) Texture analysis using morphological pattern spectrum and optimization of structuring elements. In: 10th international conference on image analysis and processing, ICIAP '99, pp 209–214
38. Mestetskiy LM (2009) Continuous morphology of the binary images. The figures. Skeletons. Circularity. Moscow Physmatlit (in Russian)
39. Shih FY, Mitchell OR (1991) Decomposition of gray-scale morphological structuring elements. *Pattern Recogn* 24(3):195–203
40. Wilkinson MHF (2002) Generalized pattern spectra sensitive to spatial information. In: 16th international conference pattern recognition, vol 1, pp 21–24
41. Urbach ER, Roerdink JBTM, Wilkinson MHF (2007) Connected shape-size pattern spectra for rotation and scale-invariant classification of gray-scale images. *IEEE Trans Pattern Anal Mach Intell* 29(2):272–285
42. van Herk M (1992) A fast algorithm for local minimum and maximum filters on rectangular and octagonal kernels. *Pattern Recogn Lett* 13(7):517–521
43. Liang EH, Wong EK (1993) Hierarchical algorithms for morphological image processing. *Pattern Recogn* 26(4):511–529
44. Park H, Chin RT (1995) Decomposition of arbitrarily shaped morphological structuring elements. *IEEE Trans Pattern Anal Mach Intell* 17(1):2–15
45. Soille P, Breen E, Jones R (1996) Recursive implementation of erosions and dilations along discrete lines at arbitrary angles. *IEEE Trans Pattern Anal Mach Intell* 18(5):562–567
46. Van Droogenbroeck M, Talbot H (1996) Fast computation of morphological operations with arbitrary structuring elements. *Pattern Recogn Lett* 17(14):1451–1460
47. Anelli G, Broggi A, Destri G (1998) Decomposition of arbitrarily shaped binary morphological structuring elements using genetic algorithms. *IEEE Trans Pattern Anal Mach Intell* 20(2):217–224
48. Van Droogenbroeck M, Buckley M (2005) Morphological erosions and openings: fast algorithms based on anchors. *J Math Imag Vis* 22:121–142
49. Gil J, Kimmel R (2002) Efficient dilation, erosion, opening and closing algorithms. *IEEE Trans Pattern Anal Mach Intell* 24(12):1606–1617
50. Urbach ER, Wilkinson MHF (2008) Efficient 2-D gray-scale morphological transformations with arbitrary flat structuring elements. *IEEE Trans Image Proc* 17(1):1–8
51. Preparata F, Sheimos M (1985) *Computational geometry: an introduction*. Springer, New York, NY, USA
52. Vizilter YV, Sidiyakin SV, Rubis A Y (2011) Calculation of morphological spectra of flat figures with the use of continuous skeletal representation. In: 15th Russian conference on mathematical methods of pattern recognition, pp 416–420 (in Russian)
53. Vizilter YV, Zheltov SY, Laretina NA (2009) Projective morphology on the basis of the operators filtering and image segmentation, computable by the method of dynamic programming. *Vestnik Comput Inf Technol* 6:18–27 (in Russian)
54. Vizilter YV, Sidiyakin SV (2012) Calculation of morphological pattern spectra of gray scale images. *Vestnik Comput Inf Technol* 4:8–17 (in Russian)
55. Sidiyakin SV (2013) Morphological pattern spectra algorithm development for digital image and video sequences analysis. PhD thesis, Moscow (in Russian)
56. Zingl A (2012) A rasterizing algorithm for drawing curves. *Multimedia und Software entwicklung*. Technikum-Wien, Wien
57. Tikhonov AN (1983) *The theory of recovery signals* Moscow, Science (in Russian)
58. Pyt'ev Y (1975) Morphological notions in problems of image analysis. Reports of USSR Academy of Science 224(6):1283–1286 (in Russian)
59. Pyt'ev Y (1975) Projection-based image analysis. *Cybernetics* 3:130–139 (in Russian)
60. Pyt'ev Y (1983) Morphological image analysis. Reports of USSR Academy of Science 3:1061–1064 (in Russian)

61. Pyt'ev Y, Chulichkov A (2010) Morphological methods for image analysis. Fizmatlit Publisher, Moscow (in Russian)
62. Pyt'ev Yu (1993) Morphological image analysis. *Pattern Recogn Image Anal* 3(1):19–28
63. Pyt'ev Y (1997) The morphology of color (multispectral) images. *Pattern Recogn Image Anal* 7(4):467–473
64. Pyt'ev Y (1998) Methods for morphological analysis of color images. *Pattern Recogn Image Anal* 8(4):517–531
65. Antonjuk V (1984) Hardware and techniques for morphological analysis of experimental multidimensional signals. Ph.D thesis (in Russian)
66. Pyt'ev Yu, Kalinin A, Loginov E, Smolovik V (1998) Morphological analysis of color images in the Chebyshev and quadratic metrics. *Pattern Recogn Image Anal* 8(2):234–235
67. Pyt'ev Y, Kalinin A, Loginov E, Smolovik V (1998) Comparison of black-and-white and Lambertian morphologies in the problem of pattern recognition. *Pattern Recogn Image Anal* 8(2):239–241
68. Pyt'ev Y, Kalinin A, Loginov E, Smolovik V (1998) On the problem of object detection by black-and-white and color morphologies. *Pattern Recogn Image Anal* 8(4):532–536
69. Chulichkov A, Grachev E, Ustinin D, Cheremukhin E (2003) Metrological measurements and signal processing in SEM based on model of signal formation. *Microelectron Eng* 69 (2–4):555–564
70. Pyt'ev YP, Falomkin II, Chulichkov AI (2006) Morphological compression of grayscale images of text. *Pattern Recogn Image Anal* 16(3):523–528
71. Evsegneev SO, Pyt'ev YP (2006) Analysis and recognition of piecewise constant texture images. *Pattern Recogn Image Anal* 16(3):398–405
72. Falomkin II, Pyt'ev YP (2007) Algorithm of adaptive morphological filtering of images. *Pattern Recogn Image Anal* 17(3):408–420
73. Pyt'ev Y, Chulichkov A (2011) Methods of morphological image analysis. Bilateral Russian–Indian scientific workshop on emerging applications of computer vision
74. Visilter Y, Zheltov S, Stepanov A (1994) Shape analysis using Pyt'ev morphologic paradigm and its use in machine vision. *SPIE Proc* 2350:163–167
75. Vizilter Y, Zheltov S (2008) Projective morphologies for image analysis. In: 9th international conference on pattern recognition and image analysis: new information technologies (PRIA-9-2008), vol 2, pp 287–290
76. Vizilter Y, Zheltov S (2010) Image segmentation in the framework of projective morphology. In: 10th international conference on pattern recognition and image analysis: new information technologies (PRIA-10-2010)
77. Vizilter YV (2011) Development of applied computer vision systems using projective morphologies and evidence-based image analysis. Bilateral Russian–Indian scientific workshop on emerging applications of computer vision (EACV-2011), pp 82–94
78. Vizilter YV, Sidiyakin SV, Rubis AY, Gorbatsevich V (2011) Skeleton-based morphological shape comparison. *Pattern Recogn Image Anal* 21(2):357–360
79. Vizilter YV, Zheltov SY (2009) The use of projective morphologies for object detection and identification in images. *J Comput Syst Sci Int* 48(2):282–294
80. Vizilter YV (2009) Design of data segmentation and data compression operators based on projective morphological decompositions. *J Comput Syst Sci Int* 48(3):415–429
81. Vizilter YV, Zheltov SY (2012) Geometrical correlation and matching of 2D image shapes. *ISPRS Ann Photogramm Remote Sens Spatial Inf Sci* 1–3:191–196
82. Pyt'ev YP (2013) Oblique projectors and relative forms in image morphology. *J Comput Math Math Phys* 53(1):21916–21937
83. Maes F, Collignon A, Vandermeulen D, Marchal G, Suetens P (1997) Multimodality image registration by maximization of mutual information. *IEEE Trans Med Imaging* 16 (2P):187–198
84. Vizilter Y, Zheltov S (2008) Projective morphologies and their application in structural analysis of digital images. *J Comput Syst Sci Int* 47(6):944–958

85. Vizilter YV, Rubis AY (2009) Metric space of image shapes. *Intell Inf Process IIP* 9:406–409 (in Russian)
86. Vizilter YV, Rubis AY (2013) Comparison of 2D image shape similarity measures. In: 11th international conference on pattern recognition and image analysis: new information technologies (PRIA-11-2013), vol 1, pp 345–348
87. Pavel M (1989) *Fundamentals of pattern recognition*. Marcel Dekker Inc., New York
88. Hough PVC (1962) Methods, means for recognizing complex patterns. U.S., patent 3069654
89. Ballard DH, Brown CM (1982) *Computer vision*. Prentice-Hall, Englewood Cliffs, New Jersey
90. Davies ER (1992) Locating objects from their point features using an optimised Hough-like accumulation technique. *Pattern Recogn* 13(2):113–121
91. Davies ER (1993) Computationally efficient Hough transform for 2-D object location. In: 4th conference on British machine vision association, vol 1, pp 259–268
92. Davies ER (2004) *Machine vision: theory, algorithms, practicalities*, 3rd edn. Academic Press, San Diego
93. Visilter Y, Zheltov S, Stepanov A (1996) Object detection and recognition using events-based image analysis. *SPIE Proc* 2823:184–195
94. Visilter Y, Zheltov S, Stepanov A (1996) Events-based image analysis for machine vision and digital photogrammetry. In: *ISPRS Proceedings of international archives of photogrammetry and remote sensing V.XXXI, Part B*, pp 898–902
95. Visilter Y, Zheltov S, Bondarenko AV, Ososkov MV, Morzhin AV (2010) *Image processing and analysis in machine vision applications*. Moscow Phismathkniga (in Russian)
96. Ballard DH (1981) Generalizing the Hough transform to detect arbitrary shapes. *Pattern Recogn* 13(2):111–122
97. Visilter Y, Gorbachevich V (2011) Morphological image analysis using dynamic programming and stacked representations. *Vestnik Comput Inf Technol* 3:7–15 (in Russian)
98. Ford L, Fulkerson D (1962) *Flows in networks*. Princeton University Press, Princeton
99. Greig D, Porteous B, Seheult A (1989) Exact maximum a posteriori estimation for binary images. *J Royal Stat Soc* 51(2):271–279
100. Boykov Y, Kolmogorov V (2003) Computing geodesics and minimal surfaces via graph cuts. *IEEE Int Conf Computer Vision (ICCV'2003)*, pp 26–33
101. Boykov Y, Kolmogorov V (2004) An experimental comparison of min-cut/max-ow algorithms for energy minimization in vision. *IEEE Trans Pattern Anal Mach Intell (PAMI)* 26(9):1124–1137
102. Darbon J, Sigelle M (2006) Image restoration with discrete constrained total variation part i: fast and exact optimization. *J Math Imaging Vision* 26(3):261–276
103. Darbon J, Sigelle M (2006) Image restoration with discrete constrained total variation part ii: levelable functions, convex and non-convex cases. *J Math Imaging Vision* 26(3):277–291
104. Zheltov SY, Vizilter YV (2004) Robust computer image analysis for flight vehicles navigation and guidance. In: 16th IFAC symposium on automatic control in aerospace, vol 2, pp 164–167
105. Vizilter YV (2008) Generalized projective morphology. *Comput Opt* 32(4):384–399 (in Russian)

Computer Vision in Control Systems-1

Mathematical Theory

Favorskaya, M.N.; Jain, L.C. (Eds.)

2015, XX, 371 p. 139 illus., 57 illus. in color., Hardcover

ISBN: 978-3-319-10652-6